PEDOSTRATIGRAPHIC INFLUENCE OF LATE-QUATERNARY SEDIMENTS AND PALEOSOLS ON HEADWALL AND SIDEWALL CANYON MORPHOLOGY IN THE ARIKAREE BREAKS, CENTRAL GREAT PLAINS

By

© 2016

Aaron Nathaniel Koop

Submitted to the graduate degree program in Geography and Atmospheric Science and the Graduate Faculty of the University of Kansas in partial fulfillment of the requirements for the degree of Master of Science.

_____

Co-Chairperson Daniel R. Hirmas

_____

Co-Chairperson William C. Johnson

_____

J. Douglas Walker

Date Defended: June 3, 2016

The Thesis Committee for Aaron N. Koop

certifies that this is the approved version of the following thesis:

PEDOSTRATIGRAPHIC INFLUENCE OF LATE-QUATERNARY SEDIMENTS AND PALEOSOLS ON HEADWALL AND SIDEWALL CANYON MORPHOLOGY IN THE ARIKAREE BREAKS, CENTRAL GREAT PLAINS

_____

Co-Chairperson Daniel R. Hirmas

_____

Co-Chairperson William C. Johnson

Date approved: June 3, 2016

ABSTRACT

Pedostratigraphy exerts considerable influence on landscape evolution and morphology in the Central Great Plains. Few locations are as well suited to undertake a soil-geomorphic study in this area as the Arikaree Breaks (hereafter 'Breaks') of northwestern Kansas and adjacent parts of Nebraska and Colorado. The Breaks are a network of impressive box canyons, which formed through erosion of a late-Quaternary loess-mantled landscape and underlying Late Cretaceous Pierre Shale and are a product of the Arikaree and Republican River watersheds eroding into the uplands of the High Plains. The primary objective of this study was to assess the influence of late-Quaternary sediments, soils, and paleosols on canyon headwall and sidewall morphology. Soil properties determined included rubification index, particle-size distribution, bulk density, dry rupture resistance, organic carbon, calcium carbonate equivalent, pH, electrical conductivity, and horizon development index. Three landform morphology properties were used in this study—surface slope, concavity, and roughness—and were measured with terrestrial laser scanning. A secondary objective was to provide detailed documentation of physical and chemical pedostratigraphic properties and pedogenic morphological development of Central Great Plains sediments (loess and sand), soils, and paleosols. Correlations and predictive statistical relationships indicated that the influence of pedostratigraphic unit and horizon-scale variability of soil properties on surface slope and concavity was muted by hydrological processes at the headwall of the canyon which appeared to control gross wall morphology and retreat as the canyon lengthened and advanced into the uplands. However, surface roughness of the headwall section was influenced by soil properties at the horizon scale. The influence of pedostratigraphic unit and horizon-scale variability of soil properties on surface slope, concavity, and roughness in the sidewall section exhibited stronger roles than in the headwall section in dictating fine-scale

morphology and sidewall retreat as the canyon widened and advanced towards other adjacent first-order canyons. Based on the relationships observed in this study, the distinctions between primary influences controlling headwall and sidewall morphology and retreat at different scales are important to consider when predicting canyon and gully development in Central Great Plains sediments, soils, and paleosols and in landscape evolution modeling of canyons and gullies in other areas where thick and highly variable pedostratigraphy is geographically extensive.

ACKNOWLEDGEMENTS

I am incredibly grateful to the Kenneth and Marian Miller family and the current landowners, Steve Miller and Janelle Miller Walter, for allowing me to conduct research on their land in the Arikaree Breaks. An enormous amount of thanks goes to the many people who have helped and supported me during the years spent working on this project. I am especially thankful to my advisors, Dr. Dan Hirmas and Dr. Bill Johnson. Dr. Hirmas provided outstanding guidance and encouragement in navigating through all aspects of this research and I am incredibly grateful for having the opportunity to learn from him. I am also very thankful for the opportunity to learn from Dr. Johnson and especially grateful for the years of funding he provided while I was working on mapping surface geology in several Kansas counties. Many thanks go to Dr. Doug Walker for his service and insights as a committee member. Many thanks also go to Dr. Jude Kastens for generously providing a space in his office area to process terrestrial laser scanning data. Thanks are also due to Dr. Kelly Kindscher for providing expertise in Arikaree Breaks plant identification. I am very grateful to Jacque Miller, Jen Glaubius, Kim Drager, Matt Myers, Eric Zautner, Dr. Alan Halfen, and Dr. Karen Willey for their help with various aspects of this work. I would also like to thank the Geography and Atmospheric Science Department, Geology Department, Kansas Geological Survey, and Kansas Biological Survey for use of facilities, transportation, and equipment. This research was generously supported by a Kollmorgen Graduate Research Scholarship and a Geological Society of America Student Research Grant. I sincerely thank Dennis Eck for assisting with numerous aspects of this project and his constant support as a truly great friend. Finally, I am sincerely and deeply thankful to my parents Faye and Cleo, my brothers Jeremy, André, and Chacour, and my fiancée Melanie Regier for their constant love and support in helping me persevere through life-changing health difficulties and challenging aspects of this project and graduate school.

TABLE OF CONTENTS

CHAPTER 1. INTRODUCTION

Previous work has shown pedostratigraphy to exert considerable influence on landscape evolution and morphology in a variety of settings (e.g., Botha et al., 1994; McAuliffe, 1994; Eppes et al., 2002; Schaetzl and Weisenborn 2004; Kemp et al., 2006). Many landscapes are a composite of various-aged landforms, parent materials, soils, erosional and depositional events, and geomorphic surfaces and, as such, stratigraphic relationships of soils and paleosols provide information on the geomorphic history of an area (Wysocki et al., 2005). This is especially true in alluvial and aeolian settings where multiple paleosols often occur (Wysocki et al., 2005). Although numerous Quaternary alluvial and aeolian pedostratigraphic records exist, few records are as extensive as loess and paleosol sequences found in regions such as the Loess Plateau of China and the North American midcontinent. These sequences provide detailed terrestrial records of climatic oscillations and influence the morphology of landscapes in these areas (Kukla, 1987; Kukla and An, 1989; Feng et al., 1994a; 1994b).

Paleosols in loess-mantled regions record paleoenvironmental conditions and indicate times of more pronounced landscape stability (Johnson et al., 2007). These stratigraphic markers, which represent former land surfaces, often occur as laterally-traceable suites of paleosols subdividing sedimentary deposits (Retallack, 1998). While well-developed paleosols have often been used to separate major loess units, these units may also contain incipient paleosols that detail the history of complex sedimentation within the deposit (Ruhe et al., 1971). This continuum of modified loess ranging from weakly developed, leached horizons to intensely weathered paleosols and pedocomplexes is characteristic of many loess sequences (Pye, 1995). Thus, thick loess pedostratigraphic records spanning ~400 ka in parts of the North American midcontinent can exhibit numerous and varying pedogenic properties (Feng et al., 1994a).

While the properties of parent materials, soil surface ages, and the intensity and duration of pedogenic processes influence the nature and distribution of soils across landscapes, soil development is continually subject to alteration by erosion and deposition events, which can lead to the exposure or burial of pedostratigraphic records (Chadwick and Graham, 2000; Wysocki et al., 2000; 2005). The effects of profile welding, truncation, rapid or slow burial, and other processes on soil properties must be considered when correlating paleosols stratigraphically and reconstructing paleoenvironmental conditions (Olson and Nettleton, 1998). These events can result in buried, exhumed, or relict paleosols exhibiting the macromorphology and micromorphology of previous and ongoing chemical, physical, and mechanical alterations (Olson and Nettleton, 1998; Nettleton et al., 2000).

In loess-mantled landscapes, processes of erosion and deposition are often expressed as extensive gully cut-and-fill cycles (Brice, 1966; Bradford et al., 1978; Porter and An, 2005). These gullies often present unique opportunities to detail thick paleosol and sediment sequences and to examine the pedostratigraphic influence on landscape evolution in these settings (e.g., Porter and An, 2005). Understanding landscape evolution in loess is particularly important for predicting gully erosion in loess-mantled regions that often contain some of the world's most agriculturally productive soils.

Pedostratigraphic Influence on Gully Morphology

In non-tectonic settings, landscape morphology is characterized by the interaction between the intensity and nature of climatic forcing throughout time and the tendencies of topographic shifts toward diffusion (Simpson and Schlunegger, 2003). The competition between colluvial and fluvial processes dictate the morphology of soil-mantled landscapes and generally result in either smoothing or incision of these landscapes (Pelletier et al., 2011). On soil-mantled

slopes, erosion can occur via slope wash, channelized fluvial erosion, or colluvial processes such as creep (Pelletier, 2012).

At the onset of erosion, surface processes such as rill and interrill dynamics, as well as subsurface processes, tend to be strongly influenced by spatially and temporally distributed soil properties such as aggregation and shear strength (Bryan, 2000). As rills transition to ephemeral channels and, ultimately, to permanent incised channels such as gullies (Bull and Kirkby, 1997), the vertical distribution of erosion resistance from contrasting soil horizons influences the size, depth, and cross-sectional morphology of these features (Bradford et al., 1978; Poesen et al., 2003). Gully headwall morphology is linked to factors such as soil, land surface, and catchment properties, and different morphologies provide indicators of certain stages of gully evolution (Oostwoud Wijdenes et al., 1999). Low soil cohesion generally results in wider and shallower gullies, while high cohesion results in slowed erosion, deeper channels, and vertical walls subject to episodic mass failures (Instanbulluoglu et al., 2005). Steep walls composed of cohesive finer-grained sediment (e.g., loess) tend to exhibit pronounced verticality when capped by more resistant, indurated units (Kirkby and Bracken, 2009). This pedostratigraphic effect is evident in gully systems where correlation of vertical wall height to substrate cohesion and material control on wall stability underscores the relationship between stratigraphy and headwall and sidewall morphology (Instanbulluoglu et al., 2005; Tucker et al., 2006).

Loess Pedostratigraphy of the Central Great Plains

A significant body of literature details research on late-Quaternary loess and intercalated paleosols mantling much of the Central Great Plains. Loess units and paleosols in this region include pre-Illinoian loess and soils, Loveland Loess and the Sangamon Soil (Illinoian), Gilman Canyon Formation (GCF) loess and soils (middle-Wisconsinan), Peoria Loess and the Brady Soil

(late-Wisconsinan), and Bignell Loess (Holocene). Early research documenting the regional loess stratigraphy (e.g., Schultz and Stout, 1945; Frye and Leonard, 1951; 1952; Reed and Dreeszen, 1965; see Welch and Hale, 1987, for a review of this work) formed the basis for numerous studies focusing on the history of loess-mantled landscapes. Many of these more recent studies established age control and paleoclimatic significance for late-Quaternary loess (e.g., Feng et al., 1994b; Maat and Johnson, 1996; Muhs et al., 1999), investigated the provenance and diversity of loess sources (e.g., Aleinikoff et al., 1999; 2008; Muhs et al., 2008), and focused specifically on middle- to late-Pleistocene (e.g., Johnson et al., 2007; Mason et al., 2007), Pleistocene-Holocene transition (e.g., Johnson and Willey, 2000; Mason et al., 2008), and Holocene loess and paleosol sequences (e.g., Mason and Kuzila, 2000; Mason et al., 2003; Miao et al., 2005). These geographically extensive and well-documented thick pedostratigraphic loess units provide the opportunity to conduct soil-geomorphic studies within a strongly established spatial and temporal context.

The Arikaree Breaks

For the Central Great Plains, few locations are as well suited to undertake a soil-geomorphic study as the Arikaree Breaks (hereafter 'Breaks'). The Breaks, located in northwestern Kansas and adjacent parts of Nebraska and Colorado, are a network of spectacular box canyons, which formed through erosion of a late-Quaternary loess-mantled landscape and underlying Late Cretaceous Pierre Shale. These box canyons are a product of the Arikaree and Republican River watersheds eroding into the uplands of the High Plains and are a unique landscape in that they (1) expose a ~400 ka-year record of late-Quaternary loess deposition and paleosol formation, (2) are one of very few locations within the Great Plains that preserve such a complete and accessible pedostratigraphic record, and (3) provide the opportunity to study

relationships between the pedostratigraphic sequence and canyon morphology. As extensive areas of the Central Great Plains are mantled by late-Quaternary loess and intercalated paleosols, research on the relationships between pedostratigraphy and canyon morphology will provide insights into the dynamics of surface processes in this region.

Breaks morphology is characterized by Holocene cycles of erosion and deposition resulting in a system of headwater tributaries entering the upper Republican River. Previous studies have documented synchronous alluvial responses throughout the Central Great Plains (e.g., Knox, 1983; Johnson and Martin, 1987; May, 1992; Mandel, 1994; Daniels and Knox, 2005) and recent work on the alluvial record of the Breaks suggested similar regional Holocene climatic changes (Willey, 2009). Willey (2009) examined records of cut-and-fill cycles and documented extensive erosion in the middle Holocene (Altithermal) beginning ~8.5 ka and ceasing 5 to 4 ka. She used optically stimulated luminescence (OSL) and AMS ^{14}C dating to study the onset of aggradation recorded in terrace remnants in lower parts of tributary canyons entering the Republican River. Remnants of a terrace (T-2) sediment package, including sequences of buried soils, preserved throughout the Breaks, have yielded a basal soil dated 3.2 to 2.9 ka, suggesting widespread system stability. Other periods of soil formation, recorded in T-2 terraces throughout the canyons, occurred ~1.8, 1.5, and 1.2 ka. Entrenchment of the T-2 likely occurred during the Medieval Warm Period (~1 ka). Resultant T-1 terraces were characterized by minimal pedogenic alteration and were cut by gullies of presumed proto-historic or historic origin (Willey, 2009).

Based on ancillary fieldwork and observations throughout the Breaks, it is evident that Miocene and Pliocene Ogallala Formation deposits once filled what were perhaps pre-existing drainage networks in Pierre Shale. Most of the Ogallala Formation deposits have been removed

(Prescott, 1953) except for some localized outcrops and lag gravels resting upon Pierre Shale. Based on laterally-traceable pedostratigraphy across the Breaks, intermittent loess deposition muted pre-existing topography and soils began developing across the area during recurrent episodes of stabilization. As mentioned previously, significant erosion likely occurred during the Holocene, incising canyons to current extents and exposing laterally-traceable sediments and paleosols. Deposition from these erosion events resulted in numerous terraces found throughout the Breaks.

Concentrated erosion and removal of remnant terraces in upper reaches of the Breaks have caused loess deposits and intercalated paleosols to be increasingly exposed from headwalls to mouths of first-order canyons where loess pedostratigraphy comes into contact with bedrock. Breaks development in these first-order canyons is influenced by laterally-traceable sequences of soils, aeolian sediments (loess and sand), paleosols, and basal Cretaceous shale. These canyons exhibit substantial removal of sediment; however, the degree to which pedostratigraphy and fine-scale vertical variability of soil properties have influenced headwall and sidewall retreat in these first-order canyons remains unknown.

The primary objective of this work was to assess the influence of late-Quaternary sediments, soils, and paleosols on canyon wall morphology. Specifically, we assessed the role of both pedostratigraphic unit and horizon-scale variability of soil properties on the development of canyon headwall and sidewall surface slope, concavity, and roughness. A secondary objective was to provide detailed documentation of physical and chemical pedostratigraphic properties and pedogenic development of Central Great Plains sediments (loess and sand), soils, and paleosols. In this work, correlations and predictive statistical relationships between soil properties and

landform morphometrics were analyzed in order to elucidate our understanding of canyon wall retreat and erosion processes in loess-mantled landscapes of the Central Great Plains.

In what follows, Chapter 2 documents materials and methods used in this research. Chapter 3 documents results and discussion of findings including summaries of first-order canyon morphology, headwall and sidewall pedostratigraphic unit and horizon-scale properties, and mean pedostratigraphic unit properties and morphometrics. Chapter 3 also includes analyses of correlations between pedostratigraphic unit properties and landform morphometrics. Analyses of predictive statistical relationships between horizon-scale properties and landform morphometrics are also included in this Chapter. Finally, Chapter 4 contains conclusions drawn from the findings of this research.

CHAPTER 2. MATERIALS AND METHODS

Study Site

Fieldwork was conducted in a first-order box canyon of the larger Hay Canyon system of the Arikaree Breaks located in Cheyenne County, Kansas (Fig. 1). The site is approximately 22.5 km north of St. Francis, Kansas just off of Parks Road/County Road 15 in a first-order canyon at 39.974595° N and 101.794384° W. The Breaks span throughout northwestern Cheyenne County, Kansas and adjacent parts of Yuma County, Colorado and Dundy County, Nebraska and are a product of the Arikaree and Republican River watersheds eroding into the uplands of the High Plains. The box canyons and gullies of the Breaks formed through erosion of a late-Quaternary loess-mantled landscape and underlying Late Cretaceous Pierre Shale and exhibit numerous cut-and-fill cycles and extensive exposures of in situ pedostratigraphy. For this study, the first-order box canyon was selected to collect terrestrial laser scanning (TLS), sedimentologic, and pedogenic data to assess pedostratigraphic influence on headwall and sidewall morphology. This particular canyon was selected based on it exhibiting representative laterally-traceable pedostratigraphy and morphology characteristic of other first-order canyons throughout the Breaks.

The Breaks have an average annual temperature of 11°C and average annual precipitation of 479 mm (High Plains Regional Climate Center, 2016). Canyon walls in this semi-arid rugged landscape are covered by sparse to moderately dense vegetation including tarragon (*Artemisia dracunculus* L.), prairie sagewort (*Artemisia frigida* Willd.), white sagebrush (*Artemisia ludoviciana* Nutt.), aromatic aster [*Symphyotrichum oblongifolium* (Nutt.) G.L. Nesom], milkvetch (*Astragalus sp.*), fourwing saltbush [*Atriplex canescens* (Pursh) Nutt.], sideoats grama [*Bouteloua curtipendula* (Michx.) Torr.], blue grama [*Bouteloua gracilis* (Willd. ex Kunth) Lag.

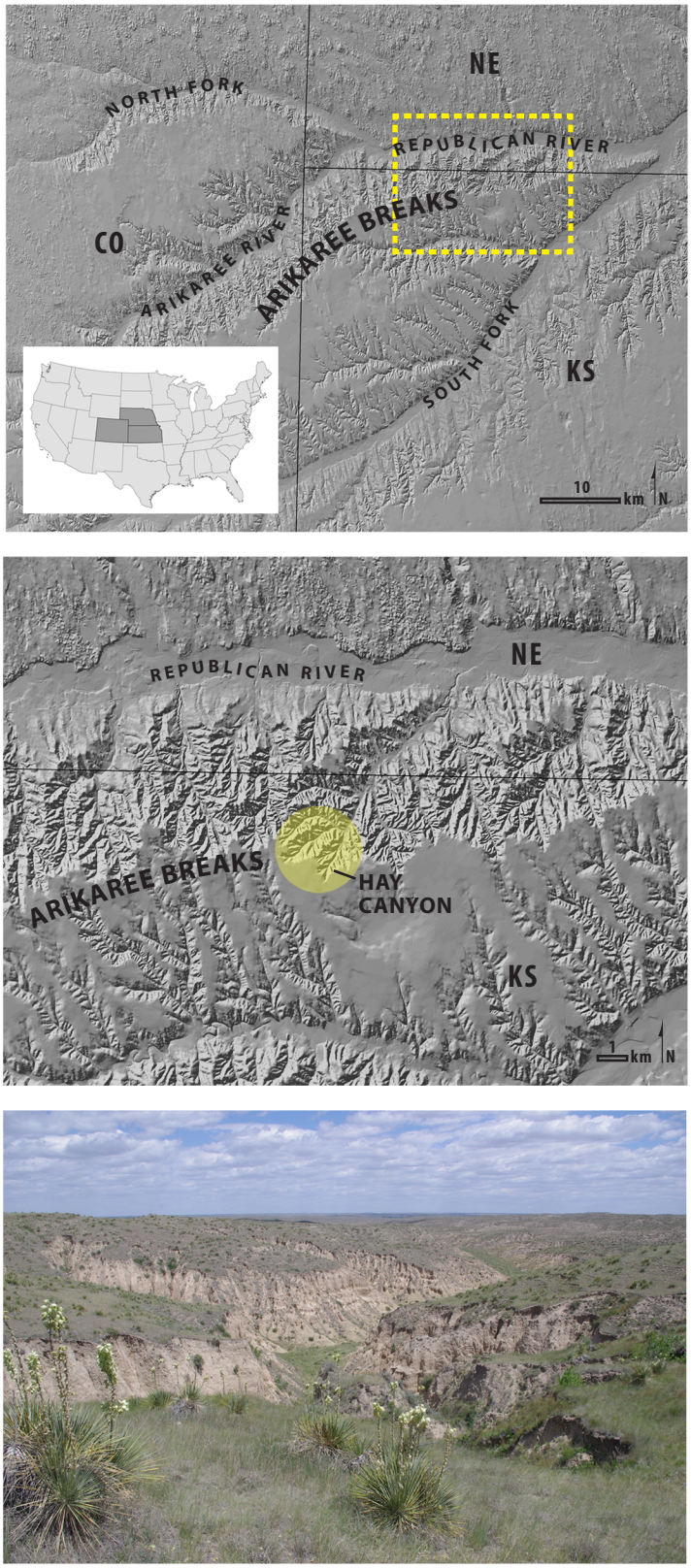

Fig. 1. Regional setting of the Arikaree Breaks and the Hay Canyon system study area. Photograph shows a view of the Hay Canyon system draining northeast to the Republican River.

ex Griffiths], white prairie clover (*Dalea candida* Michx. ex Willd.), rubber rabbitbrush [*Ericameria nauseosa* (Pall. ex Pursh) G.L. Nesom & Baird], broom snakeweed [*Gutierrezia sarothrae* (Pursh) Britton & Rusby], common sunflower (*Helianthus annuus* L.), twistspine pricklypear (*Opuntia macrorhiza* Engelm.), western wheatgrass [*Pascopyrum smithii* (Rydb.) Á. Löve], skunkbush sumac (*Rhus trilobata* Nutt.), Russian thistle (*Salsola kali* L.), sand dropseed [*Sporobolus cryptandrus* (Torr.) A. Gray], Hopi tea greenthread [*Thelesperma megapotamicum* (Spreng.) Kuntze], and soapweed yucca (*Yucca glauca* Nutt.) (USDA, 2016).

Terrestrial Laser Scanning Data Acquisition and Processing

Terrestrial laser scanning data was acquired from the headwall to mouth of one side of the first-order box canyon. A remnant terrace deposit on the opposite side of the canyon provided a flat surface from which to acquire the data. Terrestrial laser scanning data was collected using a LMS-Z620 scanner (Riegl, Horn, Austria). A portable generator was used to provide power to the scanner and a laptop while in the field. Tie-point reflectors were used to merge data from different scan positions along the canyon axis. A total of nine reflectors were placed across four different scan positions in a non-linear arrangement. The scanner was placed on a tripod on stable surfaces with a mounted camera (Nikon D300, Tokyo, Japan) and set up with line-of-sight to at least four tie-point reflectors for each scan position. RiScan Pro 1.4.3 software (Horn, Austria) was used to acquire point cloud data from each scan; data from all scan positions were merged in the field to confirm successful scanning.

Preliminary processing of the raw TLS field data was undertaken using RiScan Pro. Briefly, data points that fell outside the canyon wall were removed and true color pixels of the 2-D images from the mounted camera were assigned to the 3-D TLS point data. A series of filters and planes were applied to the point cloud data in an effort to isolate and remove

vegetation and erroneous points. Additional removal of points was undertaken in Quick Terrain Modeler 8.0.2 (Applied Imagery, Silver Springs, MD) via filters and selection tools. For this study, the primary focus was on removing vegetation points on interfluve nose slopes of the canyon headwall and sidewall. Following this removal of vegetation points, the remaining points making up the nose slopes were converted into surface models in Quick Terrain Modeler. Linear profiles following the nose slopes were generated and xyz data for these profiles were exported for pedostratigraphic and geomorphologic analyses.

Pedostratigraphic Sampling and Analyses

Prior to pedostratigraphic field descriptions and sampling, slope wash and colluvium were removed from two representative interfluve nose slopes, one from the headwall and one from the sidewall. Cleaned exposures of the headwall and sidewall nose slopes were described (i.e., horizon names and depths, boundaries, structures, ped and void surface features, effervescences, and carbonate distributions) following Schoeneberger et al. (2012). For each horizon, approximately 350 g of bulk sample was collected for color, particle-size distribution (PSD), dry rupture resistance, organic carbon (OC), inorganic carbon (CCE), pH, and electrical conductivity (EC) analyses. In addition, clods or cores were sampled from each horizon in triplicate to determine bulk density; a double-cylinder, hammer-driven core sampler (SoilMoisture Equipment Corp, Santa Barbara, CA) was used to extract core samples where possible.

In the laboratory, Munsell and L*a*b* color readings were recorded using a spectrophotometer (CM-700d, Konica Minolta, Tokyo, Japan). PSD was determined using the hydrometer method following pretreatment to remove organic matter and inorganic carbon (Bouyoucos, 1962; Soil Survey Staff, 2004). Dry rupture resistances were determined on five

replicates using a dial-gauge soil penetrometer (H-4205, Humboldt Mfg. Co., Elgin, IL). The five replicates were placed under a device to prevent the penetrometer from hitting the laboratory counter upon rupture of the peds. The penetrometer was fitted with 6.35, 10, 15, or 20 mm footing diameters depending on the rupture resistance of different peds. Footing diameters and pressure weights required to rupture the peds were recorded and used to calculate dry rupture resistance. Organic carbon and CCE were measured using a coulometer system (CM5015, UIC Inc., Joliet, IL) following Jackson and Roof (1992) and Engleman et al. (1985), respectively. Electrical conductivity and pH were determined on saturated paste extracts (Soil Survey Staff, 2004). Bulk densities were determined using a modified clod method or by weighing the known volume of the core sample for horizons where intact clods could not be sampled (Blake and Hartge, 1986; Soil Survey Staff, 2009).

Data and Statistical Analyses

All data and statistical analyses were undertaken using R 3.1.2 (R Core Team, Vienna, Austria). In addition to PSD, bulk density, dry rupture resistance, OC, CCE, pH, and EC data, rubification and horizon development indices calculated by scoring morphological properties were also used in statistical analyses. The rubification index was calculated based on dry and moist hue and chroma whereas the horizon development index (HDI) was calculated based on structure, ped and void surface features, and carbonate distribution (Table 1) (Harden, 1982; Birkeland, 1999). Structure, ped and void surface features, and carbonate distribution were all weighted equally in the HDI. In addition to field descriptions, these horizon-scale physical and chemical properties and indices were used to assess breaks between major pedostratigraphic units for the headwall and sidewall. Arithmetic depth weighted mean values for dry and moist L*a*b* color, rubification index, PSD, bulk density, OC, CCE, pH, EC, and HDI were

Table 1. Scores given to pedostratigraphic morphological properties in order to calculate rubification and horizon development indices following Harden (1982).

Property	Quantification					
Rubification†						
Points	1	-	-	-	-	18
Hue (Dry and Moist)	0.6Y	-	-	-	-	8.9YR
Highest possible score for Hue	36					
Points	1	-	-	-	-	18
Chroma (Dry and Moist)	2.6	-	-	-	-	4.3
Highest possible score for Chroma	36					
Highest possible score (Hue + Chroma)	72					
Structure‡						
Points	5	10	15	20	20	25
Grade	-	-	1	2	-	3
Size	vf	f	m	co	-	vc
Type	-	-	gr	sbk	abk	pr
Highest possible score	75					
Ped and Void Surface Features§						
Clay films and silt coats						
Points	5	10	15	20		
Amount	0	1	2	3		
Distinctness	-	ft	-	d		
Highest possible score	40					
Mn coats, Fe threads, masses and depletions						
Points	5	10	15	20		
Amount	0	1	2	3		
Size	vf	f	m	co		
Highest possible score	40					
Highest possible score (clay films and silt coats + Mn coats, Fe threads, masses and depletions)	80					
$CaCO_3$ Distribution¶						
Points	5	10	15	20	25	30
Amount	0	1	2	3	4	5
Size	-	-	vf	f	m	co
Type	-	fd	tr	c	ma	cyma
Highest possible score	90					

† Highest possible scores obtained by adding dry and moist colors.
‡ 1, weak; 2, moderate; 3, strong; vf, very fine; f, fine; m, medium; co, coarse; vc, very coarse; gr, granular; sbk, subangular blocky; abk, angular blocky; pr, prismatic.
§ 0, rare; 1, very few; 2, few; 3, common; ft, faint; d, distinct; vf, very fine; f, fine; m, medium; co, coarse.
¶ 0, rare; 1, very few; 2, few; 3, common; 4, many; 5, very many; vf, very fine; f, fine; m, medium; co, coarse; fd, finely disseminated; tr, threads; c, coats; ma, masses; cy, cylindrical.

calculated for each pedostratigraphic unit. Geometric depth weighted mean values for dry rupture resistance were also calculated for each pedostratigraphic unit. Using the TLS-derived xyz data, mean values of slope, concavity, and roughness were assessed by pedostratigraphic unit for both the headwall and sidewall. Slopes were determined from simple linear regressions fit to the elevation data for each pedostratigraphic unit. Concavity values were assessed by twice differentiating a second order polynomial fit to the data. Roughness values were calculated as the standard deviations of elevations after detrending the data using the linear fit to calculate slope.

Pedostratigraphic Unit Analyses

Depth weighted mean pedostratigraphic unit property variables (i.e., rubification index, PSD, bulk density, dry rupture resistance, OC, CCE, pH, EC, and HDI) were plotted against mean pedostratigraphic unit landform variables (i.e., slope, concavity, and roughness) for the headwall and sidewall. Pearson product moment correlation coefficients were used to examine relationships between mean pedostratigraphic unit property variables and mean pedostratigraphic unit landform variables. Correlation coefficients for both the headwall and sidewall were included for plots where either the headwall or sidewall regressions had a significant correlation coefficient ($P < 0.1$).

Horizon-Scale Analyses

Histograms of rubification index, PSD, bulk density, dry rupture resistance, OC, CCE, pH, EC, HDI, slope, concavity, and roughness data were visually inspected to assess the need for transformations among these variables. Log-transformations were applied to sand, dry rupture resistance, CCE, EC, and slope and a square root transformation was applied to roughness. In order to assess relationships between soil property variables in one location in a section and landform variables in a different location within the section, cross correlograms that displayed

the Pearson product moment correlation coefficients at various horizon lags were evaluated. These correlation coefficients, r_c, were calculated for various lags, h, following Eq. [1]:

$$r_c(h) = \frac{cov[A_i(x_i), B_i(x_i + h)]}{\sqrt{var[A_i(x_i)]}\sqrt{var[B_i(x_i + h)]}} \quad [1]$$

where A_i is the soil property variable and B_i is the landform variable associated with location x_i (Nielsen and Wendroth, 2003).

During analysis of the cross correlograms, Pearson product moment correlation coefficients that were higher or lower than one standard deviation above or below the headwall and sidewall means were used to determine horizon lags exhibiting the strongest correlations between soil property and landform variables. Cross correlograms that did not fluctuate beyond one standard deviation above or below the headwall and sidewall means were considered to have a horizon lag of zero. Headwall and sidewall horizon lags that exhibited the strongest correlations between soil property and landform variables were selected for multiple linear regression analyses.

Headwall and sidewall slope, concavity, and roughness landform variables were separated into six corresponding correlation matrices that included the most strongly correlated soil property variables at each respective horizon lag. Variance inflation factors (VIFs) were used to assess multicollinearity between the soil property variables. In this study, VIFs for the soil property variables (excluding silt due to redundancy with sand and clay) that were less than 10 were included for further analyses (Logan, 2010). After assessing multicollinearity, the remaining soil property variables associated with each of the six headwall and sidewall landform variables were z-score transformed and analyzed with multiple linear regression. The beta weights from these regressions were used to compare the relative importance of each soil

property variable to landform morphometrics. Stepwise regressions in both directions (i.e., forward and backward) were run for each of the six models in an effort to determine which soil properties were significant predictors of the landform variables. The outcomes of these models were assessed by regressing the actual headwall and sidewall slope, concavity, and roughness against predicted slope, concavity, and roughness, respectively, from the multiple linear regression equations.

CHAPTER 3. RESULTS AND DISCUSSION

First-Order Canyon Morphology

First-order canyon morphology throughout the Breaks is influenced by Pierre Shale, pre-Illinoian loess and soils, Loveland Loess and the Sangamon Soil, aeolian sand that was likely deflated from the Ogallala Formation, GCF loess and soils, Peoria Loess, and Holocene fill. Sediments and paleosols that are more resistant to erosion occur as laterally-traceable features that extend along the canyon walls but are heavily dissected by rill and gully erosion. From the headwalls to the mouths of the canyons, pedostratigraphy is increasingly truncated due to a combination of overland flow, rill, and gully erosion processes. In many cases, Holocene fill, including several buried soils, is positioned unconformably on late-Pleistocene truncated surfaces and underlying Pierre Shale. In addition to truncation of pedostratigraphy, Pierre Shale is increasingly exposed from headwalls towards mouths of the canyons. Linear profiles of interfluve nose slopes transition from steep simple convex profiles at headwalls to complex concave profiles for sidewalls approaching the canyon mouths.

Headwall Pedostratigraphic Unit and Horizon-Scale Properties

Headwall section pedostratigraphy consisted of Loveland Loess and the Sangamon Soil, aeolian sand, GCF loess and soils, Peoria Loess, and Holocene fill (Fig. 2). In what follows, summaries of headwall section pedogenic morphological descriptions and physical and chemical soil property depth profiles are discussed in an effort to set the context for pedostratigraphic influence on headwall morphology.

Holocene Fill

Headwall section Holocene fill was derived from Peoria Loess primarily via sheet erosion from upslope positions. A and Bwk horizons of the Holocene fill extended to a depth of almost 2

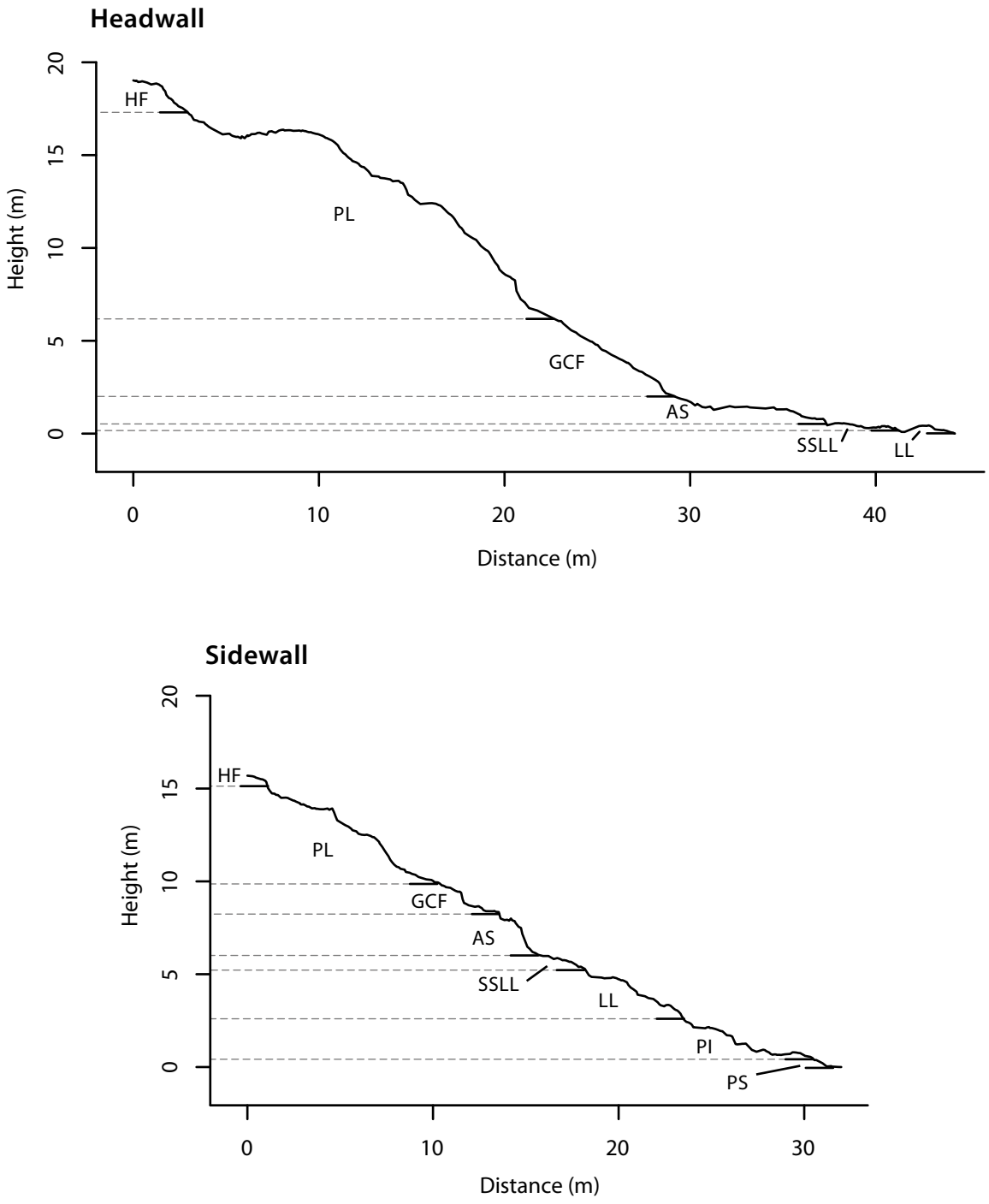

Fig. 2. Cross sections of the headwall and sidewall positions. Pedostratigraphic units for the headwall and sidewall include Holocene fill (HF), Peoria Loess (PL), Gilman Canyon Formation (GCF), aeolian sand (AS), Sangamon Soil formed in Loveland Loess (SSLL), Loveland Loess (LL), pre-Illinoian loess (PI), and Pierre Shale (PS).

m at the headwall and showed pedostratigraphic properties consistent with reworked Peoria Loess characterized by a relatively short time for soil development (Table 2) similar to that observed in T-1 terraces exhibiting minimal pedogenic alteration in the Breaks (Willey, 2009). For instance, the unit exhibited poor horizonation as indicated by an extremely narrow range of moist colors (0.3Y-0.4Y hues; 4.1-4.7 values; 2.7-3.0 chromas), loam textures throughout (sand range: 33-41%; silt range: 39-44%; clay range: 19-23%), low matrix effervescence classes (very slight and slight), and few very fine threads of $CaCO_3$ present (Table 2; Fig. 3). Horizon rubification index values (0.14-0.18), dry rupture resistances (0.04-0.16 MPa corresponding to slightly and moderately hard dry resistance classes), and CCE (2.9-3.4%) also showed little variability throughout the unit (Table 2; Fig. 3).

However, the unit showed moderate structural development in the subsoil similar to that of the Peoria Loess from which the Holocene fill originated (Table 2). Bulk density of the A horizon (1.04 g cm^{-3}) was quite low due to its origin as relatively recent slope wash but Bwk horizons within the Holocene fill, which were also formed in slope wash, had bulk densities (1.35-1.48 g cm^{-3}) which more closely approached those of the Peoria Loess pedostratigraphic unit immediately below the Holocene fill (Fig. 3). As expected, the A horizon had a higher OC content (0.77%) and OC decreased with depth to the Bwk3 horizon (0.35%) (Fig. 3). Throughout the unit, pH gradually increased with depth (7.3-7.7) as the Holocene fill approached Peoria Loess where higher pH values were more common (Fig. 3). Overall, Holocene fill EC (0.17-0.33 dS m^{-1}) had similar variability as that of the Peoria Loess (Fig. 3). However, EC of the A horizon (0.33 dS m^{-1}) appeared to indicate an increase in accumulation of salts due to percolation hanging up on a clear smooth boundary marking the transition to more development in the Bwk horizons of the subsoil (Fig. 3). Another increase in EC indicated additional accumulation of

Table 2. Pedostratigraphic morphological descriptions for the canyon headwall and sidewall.

Strat†	Horizon	Depth	Bndry§	Color		Text¶	Structure#	Resist††	P-V Feat‡‡	Efferv§§	$CaCO_3$ Dist¶¶	Notes##
				Dry	Moist							
		cm										
Canyon Headwall, Interfluve, Nose Slope (N 39.973468°, W 101.793940°)												
HF	A	0–29	cs	0.4Y 5.2/2.7	0.4Y 4.7/2.7	l	1mgr,f,msbk	sh		vs		
HF	Bwk1	29–57	gs	0.4Y 5.4/2.7	0.4Y 4.5/2.9	l	2m,cosbk	mh		sl	2vftr	
HF	Bwk2	57–112	gs	0.5Y 5.3/2.7	0.4Y 4.5/3.0	l	2m,cosbk, abk,pr	sh		sl	2vftr	
HF	Bwk3	112–188	gw	0.4Y 5.4/2.8	0.3Y 4.1/2.8	l	2m,cosbk, abk,pr	mh		sl	2vftr	
PL	Bwkb	188–251	cs	0.5Y 5.8/2.8	0.6Y 4.3/2.8	l	1cosbk-ma	mh		sl	2ftr	
PL	Bkb1	251–268	cs	0.3Y 5.8/2.9	0.4Y 4.7/3.1	l	2m,cosbk, 1mpr	sh		sl	4mc	
PL	Bkb2	268–304	cs	0.5Y 5.8/2.8	0.5Y 4.5/3.0	l	2m,co,vcsbk, 1copr	mh		sl	2ftr	
PL	B'wkb	304–336	cs	0.4Y 5.9/2.8	0.6Y 5.1/3.3	l	1cosbk	ha		sl	2vftr	
PL	B'kb	336–349	cw	0.5Y 5.9/2.8	0.4Y 4.7/3.2	l	1cosbk	mh		sl	3mc	
PL	B"wkb1	349–396	cs	0.4Y 5.9/2.8	0.4Y 4.7/3.2	l	1m,cosbk,mpr	sh		sl	2vfma,mc	
PL	B"wkb2	396–469	cs	0.3Y 6.0/3.1	0.3Y 5.2/3.5	l	1m,cosbk,mpr	mh		sl-st	2vftr,mc	
PL	B"wkb3	469–595	cs	0.2Y 6.2/3.1	0.1Y 4.7/3.5	l	2f,msbk,mpr	sh		sl	2ftr	
PL	B"wkb4	595–626	cs	0.1Y 6.1/3.2	0.1Y 4.9/3.7	l	2f,msbk, m,copr	sh		sl	1vftr	
PL	B"wkb5	626–662	cs	10.0YR 5.9/3.2	0.1Y 4.9/3.7	l	2m,cosbk, 2-3m,copr	sh		st	1vfma	
PL	B"wkb6	662–703	cs	0.2Y 6.1/3.2	0.1Y 4.9/3.6	l	2m,cosbk,pr	sh		sl-st	1vftr,ma	
PL	CBwkb	703–814‡	ds	0.1Y 6.0/3.3	0.1Y 4.7/3.5	sil	ma-1copr	sh		sl	1vftr,ma	
PL	Cb1	814‡–914‡	ds	0.1Y 6.1/3.2	0.1Y 4.8/3.6	sil	ma	sh		sl-st	0vftr	4dlpbs
PL	Cb2	914‡–1014‡	ds	0.1Y 6.1/3.2	0.1Y 5.0/3.7	sil	ma	mh		sl-st	0vftr,ma	4dlpbs
PL	Cb3	1014‡–1090	cs	10.0YR 6.1/3.3	10.0YR 5.0/3.8	sil	ma	mh		st	0vftr,ma	4dlpbs
PL	B"'wkb1	1090–1145	as	0.1Y 6.2/3.1	10.0YR 4.6/3.5	sil	1f-msbk,fpr	mh		st	0-1vftr,ma	
PL	CB'wkb	1145–1196	as	10.0YR 6.1/3.2	9.9YR 4.7/3.6	sil	ma-1copr	mh		st	0-1vftr,ma	
PL	B""wkb1	1196–1276	gs	10.0YR 6.1/3.2	9.8YR 4.7/3.6	l	1f-msbk,m, coabk,f,mpr	mh		st	2vftr,ma	
PL	B""wkb2	1276–1302	cs	9.9YR 6.1/3.2	9.7YR 4.7/3.7	sil	1m,cosbk,abk	ha		st	1vftr,ma	
GCF	2Bwkb3	1302–1345	cs	9.6YR 5.8/3.3	9.4YR 4.8/3.8	cl	ma-1copr	ha		vs	2-3ftr	
GCF	2Bwkb4	1345–1366	gs	9.4YR 5.8/3.4	9.2YR 4.8/3.9	cl	1m,coabk	ha		sl-st	2-3ftr	
GCF	2Btkb1	1366–1435	cw	9.6YR 5.9/3.3	9.3YR 4.7/4.0	cl	2m-coabk,pr	ha	0ftclfp, 2fmncp	vs	2-3ftr,ma, 3-4comarc,p	
GCF	2Btkb2	1435–1455	cs	9.5YR 6.9/2.7	9.5YR 5.3/3.6	cl	1-2m,cosbk	ha	0ftclfp, 2fmncp	ve	2-3f,mma,fd	
GCF	2B'wkb	1455–1481	cs	9.8YR 5.8/3.2	9.8YR 4.8/3.5	cl	ma-1cosbk, abk	vh	2-3ff3ma	sl	2-3vftr,ma	
GCF	2Bkb1	1481–1518	cs	9.4YR 5.7/3.5	9.1YR 4.5/4.0	cl	2m,co,vcabk	ha	2fmncp, 2-3ff3ma	vs-sl	2ftr,3comarc,p	
GCF	2Bkb2	1518–1553	cw	9.5YR 5.6/3.3	9.3YR 4.7/3.9	cl	1-2f,mpr, 1co,vcabk	vh+	0vfmncp	vs	2ftr,3cocymarc,p	
GCF	2B'tkb	1553–1572	cw	9.5YR 6.5/3.1	9.5YR 5.3/3.9	cl	2co,vcabk	vh+	0ftclfp, 2fmncp	sl	2ftr,3coma, cymarc	

Table 2. (Continued.)

Strat†	Horizon	Depth	Bndry§	Color		Text¶	Structure#	Resist††	P-V Feat‡‡	Efferv§§	$CaCO_3$ Dist¶¶	Notes##
				Dry	Moist							
GCF	2B'kb1	1572–1604	aw	9.7YR 6.0/3.1	9.7YR 4.9/3.6	cl	2co,vcabk	vh+	2fmncp, 2ff3ma	st	2ftr,4-5coma	
GCF	2B'kb2	1604–1628	cw	9.7YR 6.5/3.1	9.6YR 5.5/4.0	cl	1m-cosbk, 2f,mpr	ha	0-1fmncp	sl	3ftr,coma,fd	1ftr,machp?
GCF	2B"tkb	1628–1655	cw	9.5YR 6.2/3.5	9.4YR 4.9/4.2	cl	2fpr,m-coabk	vh	0ftclfp, 0-1fmncp	sl	4ftr	1ftr,machp?
GCF	2B"kb	1655–1691	cw	9.5YR 6.4/3.1	9.6YR 5.4/3.9	scl	1m,cosbk, abk,f,mpr	vh+	0fmncp, 2ff3tr	ve	3-4coma,fd	0fmachp?
GCF	2BCwkb	1691–1720	gs	9.7YR 6.3/3.2	9.8YR 5.3/3.6	scl	1f,msbk	vh+	0fmncp	st	2ftr,vfma	2ftrchrc?
AS	3Cb1	1720–1755	cw	9.6YR 5.9/3.3	9.7YR 5.1/3.7	ls	ma	so		sl-st	0vfma	
AS	3Cb2	1755–1807	gw	9.7YR 5.9/3.4	9.6YR 5.1/3.9	sl	ma	sh		sl-st	2vf,ftr,ma, 0cocyma	4dspbs
AS	3Cb3	1807–1867	as	9.6YR 6.0/3.3	9.5YR 5.3/4.0	ls	ma	sh	0cofed, 2.5Y 7/2	sl	1vfma	0dspbs
SSLL	4Btkb1	1867–1878	cw	9.8YR 6.4/3.0	9.7YR 5.3/3.8	cl	2fpr,m,coabk	vh+	2dclfp	ve	3f,coma	3drzm
SSLL	4Btkb2	1878–1904	cw	10.0YR 6.8/2.8	9.9YR 5.7/3.8	cl	2fpr,m,coabk	ha	2dclfp	st-ve	4f,coma	3drzm
LL	4Cb	1904–1920+		10.0YR 6.8/2.9	9.8YR 5.7/3.9	l	ma	mh		st-ve	1fma,0coma	
				Canyon Sidewall, Interfluve, Nose Slope (N 39.974595°, W 101.794384°)								
HF	A	0–13	cs	0.3Y 5.3/2.9	0.2Y 4.4/3.1	l	1-2m,cosbk	mh		vs		3coscr
HF	Bwk	13–32	as	0.2Y 5.5/2.9	0.1Y 4.5/3.3	l	1f,msbk,fpr	mh		sl	0vftr	0vcfb
PL	Bwkb1	32–48	cs	0.1Y 5.9/3.1	0.2Y 5.0/3.5	l	1-2f,msbk	mh		sl	1-2vf,ftr	
PL	Bwkb2	48–63	cw	0.1Y 6.0/3.2	0.1Y 5.0/3.6	l	1-2f,m,cosbk	sh		sl	1vftr	
PL	Bwkb3	63–105	gs	0.1Y 6.0/3.2	0.1Y 4.9/3.6	sil	1m,cosbk, abk,mpr	sh		sl	0vftr,ma	
PL	Cb1	105–156	ds	0.1Y 6.0/3.2	0.1Y 5.0/3.7	l	ma	mh		sl	0vftr,ma	
PL	Cb2	156–233	gw	0.2Y 6.1/3.1	0.2Y 5.3/3.7	l	ma	sh		sl	0vftr,ma	
PL	Cb3	233–300‡	ds	0.2Y 6.1/3.0	10.0YR 5.2/3.8	l	ma	mh		sl	0vftr,ma	
PL	Cb4	300‡–400‡	ds	10.0YR 6.1/3.3	10.0YR 5.4/3.8	sil	ma	mh		sl	0-1vf,fma	
PL	Cb5	400‡–455	ds	10.0YR 6.1/3.3	10.0YR 5.2/3.8	sil	ma	mh		sl	1ftr,ma	
PL	Cb6	455–559	as	9.9YR 6.1/3.3	10.0YR 5.1/3.8	sil	ma	mh		sl	0f,mtr	
GCF	2ABwkb	559–579	gw	9.6YR 5.6/3.1	9.5YR 4.6/3.6	cl	2co,vcabk	vh+		sl	2f,mtr,3f,mma	
GCF	2Bwkb	579–597	cw	9.5YR 5.8/3.4	9.4YR 4.9/3.8	cl	2fpr,1m,cosbk	vh+		vs-sl	3ftr,2f,mma	
GCF	2Bkb	597–619	gw	9.4YR 5.5/3.4	9.2YR 5.0/3.9	cl	2f,mabk,pr	vh+	0fmncp	vs	3-4mtr,vfma, 3cocyma,crc,p	0fmachp?
GCF	2Btkb1	619–654	cs	9.5YR 5.5/3.3	9.4YR 4.9/3.7	cl	2-3coabk, mpr	vh+	3dclfp, 0fmncp	vs	3f,mtr,ma, 4cocyma,cp	0fmachp?
GCF	2Btkb2	654–719	cs	9.3YR 6.4/2.9	9.3YR 5.2/3.8	scl	1m,cosbk,pr	vh+	0ftclfp, 0fmncp	sl	4f,m,cotr,ma	
AS	3CBkb	719–764	gs	9.6YR 6.3/3.0	9.7YR 5.3/3.6	sl	ma	mh		sl-st	2f,m,cotr,coma	
AS	3CBwkb1	764–793	gs	9.5YR 6.0/3.3	9.7YR 5.3/3.8	sl	ma	mh		vs	2vf,fma	
AS	3CBwkb2	793–856	gw	9.6YR 6.0/3.5	9.5YR 5.1/4.0	sl	1msbk	mh		sl-st	2vf,ftr,ma	

Table 2. (Continued.)

Strat†	Horizon	Depth	Bndry§	Color		Text¶	Structure#	Resist††	P-V Feat‡‡	Efferv§§	$CaCO_3$ Dist¶¶	Notes##
				Dry	Moist							
AS	3Bwkb	856–903	cw	9.4YR 6.2/3.4	9.6YR 5.6/3.9	sl	1m-cosbk	sh		sl-st	2vfma,0mma	
AS	3CB'wkb1	903–922	cw	9.5YR 6.1/3.4	9.6YR 5.1/3.8	sl	1m,cosbk	mh		sl	2vf,fma	4dspbs
AS	3CB'wkb2	922–942	cw	9.5YR 6.1/3.4	9.4YR 4.9/3.9	sl	1m,cosbk	ha		vs	2f,mtr,fma	4dspbs
SSLL	4Btkb1	942–987	cs	9.6YR 6.8/2.6	9.8YR 5.3/3.4	cl	1m,cosbk, 1-2mpr	ha	3dclfp	sl-st	4m,coma, mcyma	
SSLL	4Btkb2	987–1023	cs	9.8YR 6.7/2.9	9.8YR 5.3/3.7	cl	1f,msbk,fpr	ha	2ftclfp	sl-st	2-3ftr,3m,coma	
LL	4Cb1	1023–1100‡	ds	9.9YR 6.3/3.2	9.9YR 5.1/3.8	l	ma	mh		sl	0vfma	
LL	4Cb2	1100‡–1146	cs	9.8YR 6.4/3.3	9.7YR 5.0/4.0	l	ma	mh		sl	0vftr	
LL	4Cb3	1146–1185	cw	9.4YR 6.2/3.6	9.4YR 5.0/4.1	l	ma	mh	2dsicp	sl	0vfma	
LL	4CBwkb1	1185–1236	cs	9.3YR 6.0/3.8	9.3YR 5.2/4.2	l	ma	sh		sl	2ftr,3fma	
LL	4CBwkb2	1236–1257	cs	9.2YR 5.8/3.8	9.0YR 4.7/4.2	l	ma	so		vs-sl	2-3fma,2coma	4dlpbs
LL	4CBwkb3	1257–1274	gw	9.2YR 5.8/3.8	8.9YR 4.6/4.2	scl	ma	sh		vs	2vf,ftr,vfma	4dlpbs
LL	4CBwkb4	1274–1286	cs	9.3YR 5.7/3.9	9.1YR 4.8/4.3	scl	ma	ha		ne	3vf,fma	
PI	5Btkb1	1286–1301	aw	9.4YR 6.1/3.2	9.5YR 5.0/3.8	scl	1f,msbk	ha	2ftclfp	sl	4ftr,5fma, 0m,coma	0vftrchp?
PI	5Btkb2	1301–1319	cs	9.4YR 6.3/3.2	9.5YR 5.2/3.8	scl	1cosbk	ha	2ftclfp	sl-st	4f,mtr,3cocp,fd	0vftrchp?
PI	5Btkb3	1319–1414	gs	9.4YR 6.0/3.4	9.4YR 5.1/4.0	cl	2-3fabk,pr	ha	3dclfp	sl-st	3vftr,cocyma	0vftrchp?
PI	5Btkb4	1414–1445	cs	9.5YR 6.0/3.1	9.3YR 4.8/3.7	cl	2m,coabk, f,mpr	vh+	3dclfp	sl-st	3vftr,cocyma	0vftrchp?
PI	5CBwtkb	1445–1490	cs	9.6YR 5.9/3.5	9.5YR 4.4/3.7	cl	ma-1mpr	ha	2-3dclfp, 2mmncp	vs	2vftr,fma	
PI	5B'tkb1	1490–1502	cs	9.7YR 5.8/3.4	9.6YR 4.5/3.8	cl	ma-1cosbk	vh	2ftclfp, 0fmncp	sl-st	3vfma,2mma	
PS	6Btkb2	1502–1527	cw	9.8YR 5.7/3.7	9.7YR 4.5/3.9	cl	1f,mpr	vh	2ftclfp, 0fmncp	sl	4f,mtr,ma, 2coma	2mpb
PS	6Crtk	1527–1546+		9.8YR 5.9/3.5	9.5YR 4.3/4.0	c	ma	ha	2ftclfr, 2-3fmncr, 2-3ff3mar	st	4mcr	2mpb,sapr

† Strat, Stratigraphy; HF, Holocene fill; PL, Peoria Loess; GCF, Gilman Canyon Formation; AS, aeolian sand; SSLL, Sangamon Soil formed in Loveland Loess; LL, Loveland Loess; PI, pre-Illinoian loess; PS, Pierre Shale.

‡ Horizon depth arbitrarily broken for describing and sampling.

§ Bndry, Boundary; a, abrupt; c, clear; g, gradual; d, diffuse; s, smooth; w, wavy.

¶ Text, Texture; ls, loamy sand; sl, sandy loam; l, loam; sil, silt loam; scl, sandy clay loam; cl, clay loam; c, clay.

1, weak; 2, moderate; 3, strong; vf, very fine; f, fine; m, medium; co, coarse; vc, very coarse; gr, granular; sbk, subangular blocky; abk, angular blocky; pr, prismatic; ma, massive.

†† Resist, Dry Rupture Resistance; so, soft; sh, slightly hard; mh, moderately hard; ha, hard; vh, very hard; +, 1 to 3 of the 5 peds used to calculate mean dry rupture resistance did not rupture at the maximum limit of force applied (107.8 N) by the soil penetrometer.

‡‡ P-V Feat, Ped and Void Surface Features; 0, rare; 1, very few; 2, few; 3, common; ft, faint; d, distinct; vf, very fine; f, fine; m, medium; co, coarse; clf, clay films; sic, silt coats; mnc, manganese coats; f3tr, iron threads; f3ma, iron masses; fed, iron depletions; p, on ped surfaces; rc, in root channels; r, on weathered shale.

§§ Efferv, Matrix Effervescence; ne, noneffervescent; vs, very slightly effervescent; sl, slightly effervescent; st, strongly effervescent; ve, violently effervescent.

¶¶ Dist, Distribution; 0, rare; 1, very few; 2, few; 3, common; 4, many; 5, very many; vf, very fine; f, fine; m, medium; co, coarse; fd, finely disseminated; tr, threads; c, coats; ma, masses; cy, cylindrical; p, on ped surfaces; rc, in root channels; r, on weathered shale.

0, rare; 1, very few; 2, few; 3, common; 4, many; d, distinct; vf, very fine; f, fine; m, medium; co, coarse; vc, very coarse; tr, threads; ma, masses; ch, charcoal; p, on ped surfaces; rc, in root channels; rzm, reddish zones in matrix; scr, surface crust; fb, faunal burrow; l, loess; s, sand; pbs, primary bedding structures; pb, pebbles; sap, saprolitized; r, shale.

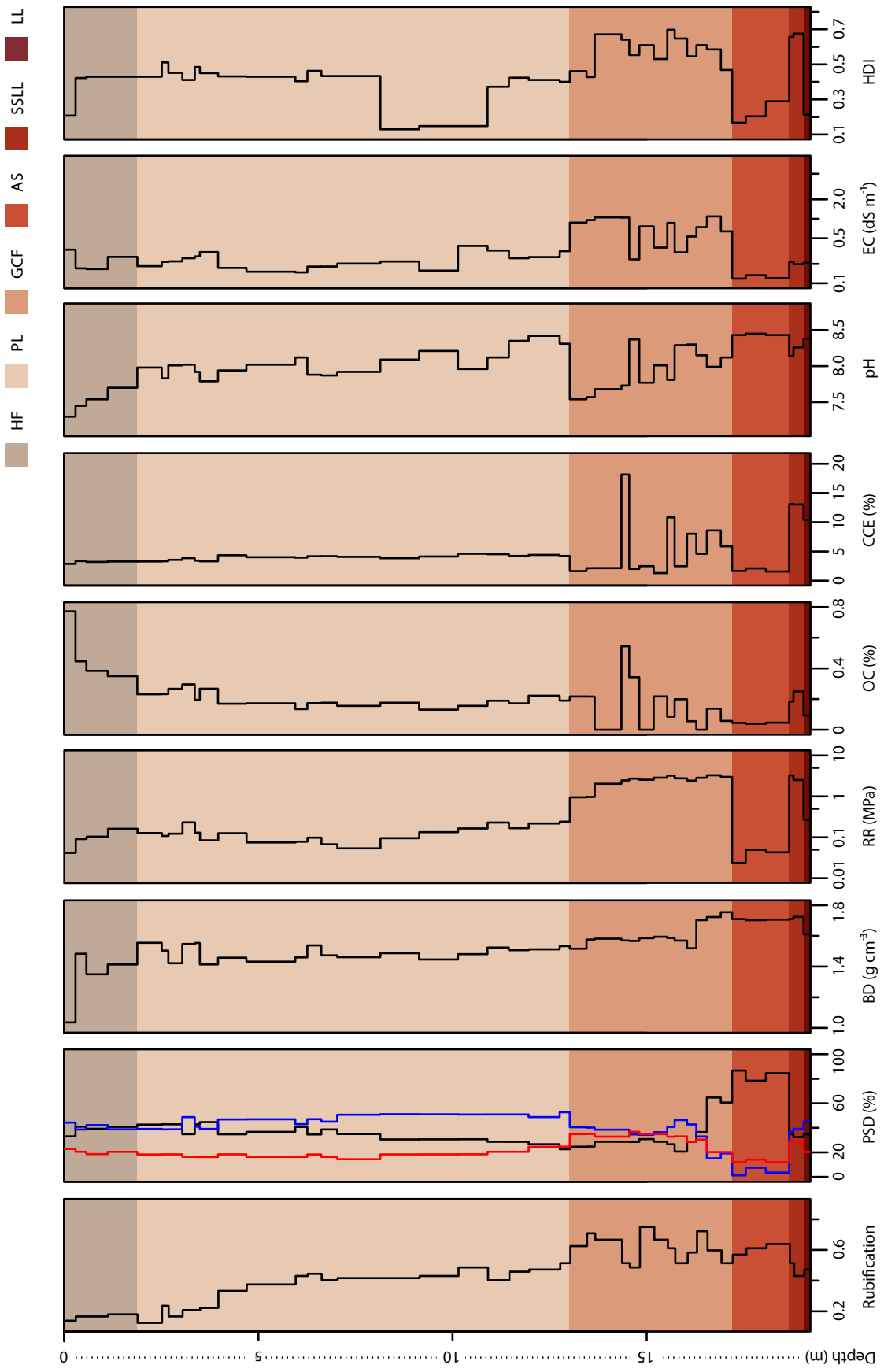
LL
SSLL
AS
GCF
PL
HF
Depth (m)
0
5
10
15
Rubification
0.2
0.6
PSD (%)
0
20
60
100
BD (g cm-3)
1.0
1.4
1.8
RR (MPa)
0.01
0.1
1
10
OC (%)
0
0.4
0.8
CCE (%)
0
5
10
15
20
pH
7.5
8.0
8.5
EC (dS m-1)
0.1
0.5
2.0
HDI
0.1
0.3
0.5
0.7

Fig. 3. Depth profiles of rubification, particle-size distribution (PSD), bulk density (BD), dry rupture resistance (RR), organic carbon (OC), calcium carbonate equivalent (CCE), pH, electrical conductivity (EC), and horizon development index (HDI) for the canyon headwall. Colors refer to pedostratigraphic units including Holocene fill (HF), Peoria Loess (PL), Gilman Canyon Formation (GCF), aeolian sand (AS), Sangamon Soil formed in Loveland Loess (SSLL), and Loveland Loess (LL).

salts occurring in the Bwk3 horizon (0.26 dS m^{-1}) right above a gradual wavy boundary where Holocene fill had buried and welded into truncated Peoria Loess and initial properties of the Peoria Loess unit (e.g., massive features and increased bulk density) had slowed percolation between pedostratigraphic units (Table 2; Fig. 3). In addition, HDI values (0.21-0.43) increased with depth and indicated a progression towards similar soil development as that of parts of the underlying Peoria Loess (Fig. 3).

Peoria Loess

As mentioned, a gradual wavy boundary between the Holocene fill and Peoria Loess exhibited processes of welding into the previously truncated surface of the Bwkb horizon (Table 2). Beginning with this horizon, Peoria Loess of the headwall section extended from nearly 2 m to 13 m in depth and was massive in nature but also exhibited properties consistent with weak to moderate soil development (Table 2) that were similarly observed in numerous other studies (e.g., Maat and Johnson, 1996; Muhs et al., 1999; 2008). For example, from a depth of ~2 to 7 m, weak to moderate soil development in inherently massive loess was exhibited in a series of Bwkb and Bkb horizons with a somewhat narrow range of moist colors (0.1-0.6Y hues; 4.3-5.2 values; 2.8-3.7 chromas), loam textures (sand range: 35-45%; silt range: 39-49%; clay range: 16-18%), and predominantly weak to moderate structural development (Table 2; Fig. 3). Except for the dry rupture resistance of the B'wkb horizon at a depth of 3.0 to 3.4 m (0.23 MPa corresponding to a hard dry resistance class), resistances for Bwkb and Bkb horizons from ~2 to 7 m (0.07-0.13 MPa corresponding to slightly and moderately hard dry resistance classes) showed little variability (Table 2; Fig. 3). Likewise, little variability was exhibited in matrix effervescences (predominantly slight and some slight to strong effervescence classes) and CCE (3.3-4.4%) for this depth range (Table 2; Fig. 3).

Several properties of horizons for the depth spanning ~2 to 7 m more clearly highlighted different aspects of the weak to moderate soil development occurring in massive loess (Table 2). For instance, in general, rubification index values (0.13-0.44) gradually increased with depth while OC contents (0.13-0.30%) gradually decreased (Fig. 3). In addition, bulk densities (1.41-1.55 g cm^{-3}), pH (7.8-8.1), EC (0.15-0.31 dS m^{-1}), and HDI values (0.40-0.51) of Bwkb and Bkb horizons spanning this depth showed more variability associated with pedogenic processes that modified this massive loess (Fig. 3). Electrical conductivities gradually increased from ~2 to almost 4 m perhaps indicating an increase in accumulation of salts as percolating water was hung up on Bkb and associated Bwkb horizons (Table 2; Fig. 3). It should be noted that pH and EC exhibited an inverse relationship at this site but the dynamics of this relationship were unclear (Fig. 3). With respect to HDI values, variability was mainly attributed to slightly higher values for Bkb horizons due to moderate structural development and/or increased $CaCO_3$ distribution (very few to many amounts) (Table 2; Fig. 3).

At approximately 7 m, a clear smooth boundary marked a transition to predominantly massive loess continuing to a depth of almost 11 m (Table 2). A CBwkb horizon and several Cb horizons (arbitrarily broken for descriptions and sampling with diffuse smooth boundaries) exhibited little variability as indicated by an extremely narrow range of moist colors (10.0YR-0.1Y hues; 4.7-5.0 values; 3.5-3.8 chromas), silt loam textures (sand range: 31-35%; silt range: ~51%; clay range: 14-18%), and many distinct loess primary bedding structures in Cb horizons (Table 2; Fig. 3). Rubification index values (0.42-0.49) and dry rupture resistances (0.05-0.16 MPa corresponding to slightly and moderately hard dry resistance classes) increased only slightly with depth for these horizons and bulk densities (1.45-1.49 g cm^{-3}), OC (0.13-0.18%), and CCE (3.8-4.6%) showed little variability in these massive parts of the Peoria Loess (Table 2;

Fig. 3). Matrix effervescence gradually increased from the CBwkb horizon to the Cb3 horizon (slight through strong effervescence classes) but $CaCO_3$ distribution was reduced to rare to very few amounts (Table 2). Some variability in the massive loess was present with respect to pH (7.9-8.2) and more so with EC (0.16-0.38 dS m^{-1}) as there was a moderate increase in EC (0.38 dS m^{-1}) and a decrease in pH (8.0) for the Cb3 horizon at a clear smooth boundary that transitioned into increased underlying soil development (Table 2; Fig. 3). As previously mentioned, it was unclear why pH and EC exhibited an inverse relationship at this site. As expected, after the HDI value of the CBwkb horizon (0.43), HDI values of Cb horizons (0.13-0.15) dropped substantially indicating an overall lack of soil development (Table 2; Fig. 3).

The lowermost part of the headwall Peoria Loess extended from almost 11 to 13 m in depth and exhibited a return to weak to moderate soil development with some properties of the massive loess still present (Table 2). This lowermost part was composed of Bwkb horizons along with a CBwkb horizon and was characterized by a narrow range of moist colors (9.7-10.0YR hues; 4.6-4.7 values; 3.5-3.7 chromas), mostly silt loam textures (sand range: 23-29%; silt range: 49-53%; clay range: 20-25%), and massive to weak structural development (Table 2; Fig. 3). In addition to strong matrix effervescences but rare to few $CaCO_3$ distribution amounts, rubification index values (0.40-0.51), bulk densities (1.51-1.53 g cm^{-3}), dry rupture resistances (0.16-0.24 MPa corresponding to moderately hard and hard dry resistance classes), OC (0.17-0.22%), CCE (4.2-4.5%), pH (8.1-8.4), EC (0.25-0.32 dS m^{-1}), and HDI values (0.37-0.42) all showed little variability indicating weak to moderate soil development in what was once massive loess (Table 2; Fig. 3). Lastly, abrupt smooth boundaries between the B'"wkb1 and CB'wkb horizons and the CB'wkb and B""wkb1 horizons at depths of 11.45 m and 11.96 m, respectively, indicated what

were perhaps early episodes of somewhat rapid loess deposition in the lowermost part of the Peoria Loess pedostratigraphic unit (Table 2).

Gilman Canyon Formation

Gilman Canyon Formation loess and soils of the headwall section spanned from ~13 to over 17 m in depth and exhibited properties consistent with horizonation derived from pedogenic processes modifying previous cumulic soil development (Table 2) similar to findings from other studies documenting the GCF pedocomplex (e.g., Reed and Dreeszen, 1965; Feng et al., 1994a; Johnson et al., 2007). For instance, OC (0-0.54%) and CCE (1.3-18.2%) were quite variable and, for the most part, increases and decreases of values corresponded to buried soil and loess remnants, respectively, as these properties were strong indicators of cumulic sequences subjected to continued alteration by pedogenic processes (Fig. 3). Likewise, due to the cumulic nature of the GCF, moist colors (9.1-9.8YR hues; 4.5-5.5 values; 3.5-4.2 chromas), rubification index values (0.49-0.75), pH (7.5-8.4), EC (0.24-1.09 dS m^{-1}), and HDI (0.43-0.70) were all quite variable but this underlying variability has undergone strong pedogenic alteration that has resulted in profile welding and, thus, indistinct definition of the sequences (Table 2; Fig. 3). Similarly, the presence and variability of ped and void surface features (rare to common amounts between 13.7 and 17.2 m), matrix effervescences (very slight to violent effervescence classes), and $CaCO_3$ distribution (few to very many amounts) also exhibited initial cumulic soil development coupled with and altered by continued pedogenic modification (Table 2). In addition, higher EC values for several Btkb and some Bkb horizons appeared to indicate increases in accumulation of salts due to percolating waters likely being hung up throughout the GCF (Fig. 3). As mentioned before, it was unclear why pH and EC were inversely related at this site (Fig. 3).

The headwall GCF exhibited predominantly weak to moderate structural development but massive features were also present in two horizons (2Bwkb3 and 2B'wkb) of the unit (Table 2). Although cumulic and massive features were still present throughout the unit, continued pedogenic modification of the GCF was exhibited in clay loam textures (sand range: 21-37%; silt range: 33-46%; clay range: 29-37%) from ~13 to 16.6 m and sandy clay loam textures (sand range: 61-65%; silt range: 15-19%; clay range: 20%) from 16.6 to 17.2 m as the unit approached the underlying aeolian sand (Table 2; Fig. 3). From ~13 to 16.3 m, GCF bulk densities (1.52-1.59 g cm^{-3}) showed little variability until substantially increasing from 16.3 to 17.2 m (1.70-1.75 g cm^{-3}) as the unit approached the underlying aeolian sand (Fig. 3). The uppermost two horizons of the GCF unit spanned ~13 to 13.7 m and dry rupture resistances of these horizons (0.94 and 0.96 MPa corresponding to hard dry resistance classes) showed substantial increases from that of the overlying Peoria Loess (Fig. 3). Another substantial increase in dry rupture resistance occurred within the GCF unit beginning at 13.7 m and this marked a transition to higher dry rupture resistances (2.01-3.24 MPa corresponding to hard and very hard dry resistance classes) and little variability until the lowermost part of the unit at 17.2 m (Fig. 3).

Aeolian Sand

Aeolian sand of the headwall section spanned from 17.2 to ~18.7 m in depth and this massive unit was composed of three Cb horizons with a narrow range of moist colors (9.5-9.7YR hues; 5.1-5.3 values; 3.7-4.0 chromas) and loamy sand and sandy loam textures (sand range: 78-87%; silt range: 1-8%; clay range: 12-14%) (Table 2; Fig. 3) and was similarly documented below the GCF at other sites in Kansas and Nebraska (Feng et al., 1994b; Pye et al., 1995). The unit had slight and slight to strong matrix effervescences, rare, very few, and few $CaCO_3$ distribution amounts and the 3Cb2 and 3Cb3 horizons exhibited many and rare distinct sand

primary bedding structures, respectively (Table 2). Aeolian sand rubification index values (0.57-0.64) were similar to those of the overlying GCF and bulk densities (1.70-1.71 g cm^{-3}) were similar to the bottom three horizons of the GCF but both of these aeolian sand properties exhibited much less variability (Fig. 3). Dry rupture resistances (0.02-0.05 MPa corresponding to soft and slightly hard dry resistance classes), OC (0.04-0.05%), CCE (1.6-2.1%), pH (8.4-8.5), and EC (0.12-0.13 dS m^{-1}) also exhibited little variability and except for pH, values were, for the most part, lower than those of the overlying GCF (Table 2; Fig. 3). Low EC values in the aeolian sand indicated that salts were most likely easily removed by percolation throughout the unit (Fig. 3). Correspondingly, pH values were higher throughout the aeolian sand unit (Fig. 3). In addition, HDI values (0.17-0.29) were much lower than those of the overlying GCF but gradually increased with depth and in the bottom horizon (3Cb3) of the unit, rare coarse iron depletions and an abrupt smooth boundary at 18.67 m indicated that percolating waters were perhaps slowed and hung up at the transition into the Sangamon Soil (Table 2; Fig. 3).

Sangamon Soil

The headwall Sangamon Soil unit spanned from ~18.7 to over 19 m in depth and was composed of two Btkb horizons exhibiting properties consistent with well-developed horizonation derived from pedogenic processes modifying Loveland Loess (Table 2) and was similarly described in numerous other studies (e.g., Brice, 1966; Johnson et al., 2007; Mason et al., 2007). In addition, Sangamon Soil moist colors (9.7-9.9YR hues; 5.3-5.7 values; 3.8 chromas), rubification index values (0.43-0.51), and common distinct reddish zones in the matrix of the unit indicated the likely presence of reducing conditions in the past (Table 2; Fig. 3). Rubification index values of the Sangamon Soil were also lower, for the most part, than those of the overlying GCF and aeolian sand units perhaps indicating the presence of reducing conditions

(Fig. 3). The Sangamon Soil unit of the headwall section was well-developed with clay loam textures (sand range: 32-35%; silt range: 37-39%; clay range: 28-29%), moderate structural development, few distinct clay films on ped surfaces, strong to violent and violent matrix effervescence classes, and common and many $CaCO_3$ distribution amounts (Table 2; Fig. 3).

Sangamon Soil bulk densities (1.71-1.72 g cm^{-3}) were similar to those of lower parts of the overlying GCF as well as the aeolian sand unit (Fig. 3). Sangamon Soil dry rupture resistances (2.49-3.22 MPa corresponding to hard and very hard dry resistance classes) were similar to those of the GCF but increased dramatically from those of the aeolian sand unit (Table 2; Fig. 3). Similar to the bulk densities and dry rupture resistances of this unit, OC (0.18-0.25%), CCE (13.0-13.1%), pH (8.1-8.3), EC (0.20-0.22 dS m^{-1}), and HDI (0.66-0.68) showed little variability and represented pedogenic processes resulting in a well-developed Sangamon Soil in the headwall section (Fig. 3). Lastly, OC and CCE of the Sangamon Soil increased substantially from that of the overlying aeolian sand and underlying Loveland Loess and an increase in EC appeared to indicate accumulation of salts due to percolating waters hung up at the contact of the unit (Fig. 3).

Loveland Loess

Loveland Loess of the headwall section spanned from ~19 to over 19.2 m in depth and this massive unit was composed of one Cb horizon resting on the floor of the first-order canyon (Table 2). This lowermost horizon of the headwall section exhibited properties consistent with massive loess with a similar moist color (9.8YR hue; 5.7 value; 3.9 chroma) and rubification index value (0.47) as that of the overlying Sangamon Soil horizons, a loam texture (sand: 35%; silt: 45%; clay: 20%), strong to violent matrix effervescence, and rare and very few $CaCO_3$ distribution amounts (Table 2; Fig. 3). Bulk density (1.61 g cm^{-3}) and dry rupture resistance

(0.27 MPa corresponding to a moderately hard dry resistance class) of the Loveland Loess Cb horizon were lower than bulk densities and dry rupture resistances of the Sangamon Soil horizons (Table 2; Fig. 3). Organic carbon (0.09%) and CCE (10.4%) of the Cb horizon were also lower than OC and CCE of the overlying Sangamon Soil horizons (Fig. 3). In addition, pH (8.4) and EC (0.21 dS m^{-1}) of the Cb horizon were similar to pH and EC of the Sangamon Soil horizons (Table 2; Fig. 3). Finally, HDI of the Cb horizon (0.21) was indicative of the upper part of a massive loess unit with an overall lack of soil development and this value was similar to those found in massive parts of the Peoria Loess and aeolian sand units (Fig. 3).

Sidewall Pedostratigraphic Unit and Horizon-Scale Properties

Pedostratigraphy of the sidewall section consisted of Pierre Shale, pre-Illinoian loess and soils, Loveland Loess and the Sangamon Soil, aeolian sand, GCF loess and soils, Peoria Loess, and Holocene fill (Fig. 2). Similar to the headwall section, summaries of sidewall section pedogenic morphological descriptions and physical and chemical soil property depth profiles are discussed below in an effort to set the context for pedostratigraphic influence on sidewall morphology.

Holocene Fill

Holocene fill of the sidewall section extended to a depth of 32 cm and was composed of an A horizon and a Bwk horizon that rested unconformably on truncated Peoria Loess as exhibited by an abrupt smooth lower boundary (Table 2). In addition, a common coarse surface crust was present in the A horizon as well as a rare very coarse faunal burrow in the Bwk horizon (Table 2). This unit was derived from Peoria Loess primarily via sheet erosion from upslope positions and exhibited pedostratigraphic properties consistent with a relatively short time for soil development. The unit showed poor horizonation as indicated by a very narrow range of

moist colors (0.1-0.2Y hues; 4.4-4.5 values; 3.1-3.3 chromas), loam textures (sand range: 33-35%; silt range: 44-45%; clay range: 21-22%), weak to moderate structural development, low matrix effervescence classes (very slight and slight), and the presence of rare very fine threads of $CaCO_3$ in the Bwk horizon (Table 2; Fig. 4).

Bulk densities (1.29-1.32 g cm^{-3}), dry rupture resistances (0.07-0.18 MPa corresponding to moderately hard dry resistance classes), pH (7.9-8.0), and EC (0.17-0.22 dS m^{-1}) all showed little variability and these properties were also consistent with a short time for soil development in reworked Peoria Loess parent material (Table 2; Fig. 4). Rubification index values (0.26-0.32), CCE (2.55-4.10%), and HDI (0.24-0.34) all increased with depth and approached similar values as that of the underlying Peoria Loess pedostratigraphic unit (Fig. 4). As expected, Holocene fill OC (0.55-0.78%) decreased with depth in the unit (Fig. 4).

Peoria Loess

Sidewall section Peoria Loess spanned from 32 cm to over 5.6 m in depth and was composed of three Bwkb horizons followed by six Cb horizons (Table 2). The three Bwkb horizons extended from 32 to 105 cm in depth and exhibited somewhat poor horizonation as indicated by a very narrow range of moist colors (0.1-0.2Y hues; 4.9-5.0 values; 3.5-3.6 chromas), loam (Bwkb1 and Bwkb2 horizons) and silt loam (Bwkb3 horizon) textures (sand range: 29-37%; silt range: 42-51%; clay range: 16-23%), weak to moderate structural development, slight matrix effervescences, and rare, very few, and few $CaCO_3$ distribution amounts (Table 2; Fig. 4). Rubification index values (0.38-0.42), bulk densities (1.41-1.49 g cm^{-3}), dry rupture resistances (0.10-0.16 MPa corresponding to slightly and moderately hard dry resistance classes), CCE (4.2-4.7%), EC (0.19-0.21 dS m^{-1}), and HDI (0.38-0.39) all showed little variability and were consistent with weakly defined horizonation and soil development

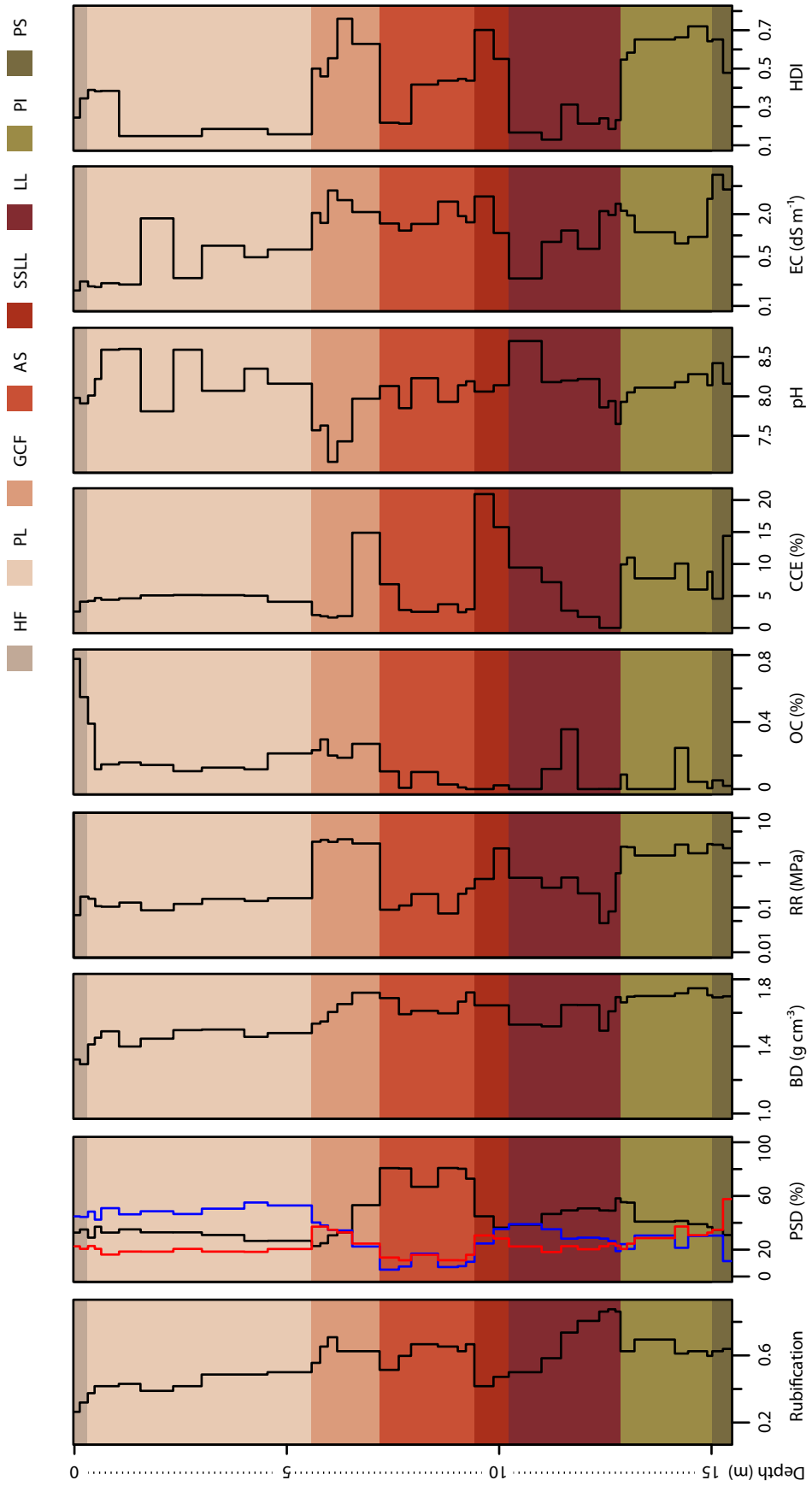
PS
PI
LL
SSLL
AS
GCF
PL
HF
Depth (m)
0
5
10
15
Rubification
0.2
0.6
PSD (%)
0
20
60
100
BD (g cm-3)
1.0
1.4
1.8
RR (MPa)
0.01
0.1
1
10
OC (%)
0
0.4
0.8
CCE (%)
0
5
10
15
20
pH
7.5
8.0
8.5
EC (dS m-1)
0.1
0.5
2.0
HDI
0.1
0.3
0.5
0.7

Fig. 4. Depth profiles of rubification, particle-size distribution (PSD), bulk density (BD), dry rupture resistance (RR), organic carbon (OC), calcium carbonate equivalent (CCE), pH, electrical conductivity (EC), and horizon development index (HDI) for the canyon sidewall. Colors refer to pedostratigraphic units including Holocene fill (HF), Peoria Loess (PL), Gilman Canyon Formation (GCF), aeolian sand (AS), Sangamon Soil formed in Loveland Loess (SSLL), Loveland Loess (LL), pre-Illinoian loess (PI), and Pierre Shale (PS).

(Table 2; Fig. 4). In addition, Bwkb1 OC (0.39%) decreased to 0.12-0.15% for the Bwkb2 and Bwkb3 horizons and pH (8.0-8.6) was inversely related to EC and somewhat variable as it gradually increased in the uppermost part of the Peoria Loess unit (Fig. 4).

The sidewall Peoria Loess unit continued to extend from ~1 to 5.6 m in depth in a series of six Cb horizons (Cb3, Cb4, and Cb5 horizons were arbitrarily broken for descriptions and sampling with diffuse smooth boundaries) formed in massive loess (Table 2). These horizons exhibited an overall lack of soil development with a narrow range of moist colors (10.0YR-0.2Y hues; 5.0-5.4 values; 3.7-3.8 chromas), loam (Cb1, Cb2, and Cb3 horizons) and silt loam (Cb4, Cb5, and Cb6 horizons) textures (sand range: 27-35%; silt range: 46-55%; clay range: 18-21%), slight matrix effervescences, and rare to very few $CaCO_3$ distribution amounts (Table 2; Fig. 4). After initially decreasing from the Cb1 to the Cb2 horizon, rubification index values (0.39-0.50) increased slightly with depth while bulk densities (1.40-1.50 g cm^{-3}), dry rupture resistances (0.09-0.16 MPa corresponding to slightly and moderately hard dry resistance classes), CCE (4.1-5.2%), and HDI (0.15-0.19) exhibited little variability throughout the Cb horizons of the massive loess (Table 2; Fig. 4). Organic carbon (0.11-0.21%) of the massive loess also showed little variability until substantially increasing from 4.6 to 5.6 m in the Cb6 horizon just above the GCF (Table 2; Fig. 4). Substantial variability in the massive loess was present with respect to pH (7.8-8.6) and EC (0.20-1.74 dS m^{-1}) as these properties exhibited an inverse relationship and higher EC values indicated reduced hydraulic conductivity and accumulation of salts in the Cb2 horizon (1.6-2.3 m) as well as in the Cb4, Cb5, and Cb6 horizons (3.00-5.59 m) overlying an abrupt smooth boundary that transitioned into the GCF (Table 2; Fig. 4).

Gilman Canyon Formation

Gilman Canyon Formation loess and soils of the sidewall section were truncated in the past (as indicated by an abrupt smooth boundary at 5.6 m) and this unit spanned 5.6 to 7.2 m in depth with properties consistent with horizonation derived from pedogenic processes modifying previous cumulic soil development (Table 2). Although moist colors (9.2-9.5YR hues; 4.6-5.2 values; 3.6-3.9 chromas) were somewhat narrow in range, moderately to strongly developed GCF horizonation was exhibited in weak to moderate and some strong structural development, clay loam textures of the upper four horizons (sand range: 23-33%; silt range: 34-40%; clay range: 33-37%), and a sandy clay loam texture in the lowermost 2Btkb2 horizon (sand: 53%; silt: 22%; clay: 25%) overlying the aeolian sand unit (Table 2; Fig. 4). Moderately to strongly developed GCF horizonation was also exhibited in rare and common ped and void surface features, very slight to slight matrix effervescences, and few, common, and many $CaCO_3$ distribution amounts (Table 2).

As mentioned, the sidewall GCF exhibited cumulic soil development subjected to continued modification by pedogenic processes and profile welding as well as alteration by truncation and removal of horizons. These processes resulted in increased variability of properties from horizon to horizon. For instance, variability of rubification index values (0.56-0.71), OC (0.19-0.30%), pH (7.2-8.0), EC (1.50-4.33 dS m^{-1}), and HDI (0.46-0.76) indicated the occurrence of pedogenic processes modifying cumulic sequences (Fig. 4). Higher EC values in the uppermost 2ABwkb horizon as well as underlying Bkb and Btkb horizons appeared to indicate increased accumulation of salts due to percolation being hung up throughout the GCF (Table 2; Fig. 4). Electrical conductivities and pH values of horizons exhibited an inverse relationship throughout the GCF unit although the dynamics of this relationship continued to

remain unclear (Fig. 4). In addition, from 5.9 to 6.5 m, CCE (1.6-2.0%) showed little variability but increased substantially to 14.9% in the 2Btkb2 horizon between 6.5 and 7.2 m (Table 2; Fig. 4). Although substantial horizon to horizon variability of soil properties was exhibited throughout the GCF of the sidewall section, bulk densities (1.54-1.72 g cm^{-3}) showed less variability and gradually increased with depth perhaps in part due to increased consolidation from the weight of overlying sediments and soils (Fig. 4). Lastly, dry rupture resistances (2.71-3.37 MPa corresponding to very hard dry resistance classes) exhibited the least amount of variability of all of the soil properties perhaps due to overall stronger pedogenic processes (e.g., translocation) occurring across all horizons of the unit (Table 2; Fig. 4).

Aeolian Sand

Sidewall section aeolian sand spanned from 7.2 to 9.4 m in depth and was composed of CBkb, CBwkb, and Bwkb horizons exhibiting little to weak soil development but moderate variability of properties throughout the unit with a somewhat narrow range of moist colors (9.4-9.7YR hues; 4.9-5.6 values; 3.6-4.0 chromas), sandy loam textures (sand range: 67-81%; silt range: 5-17%; clay range: 12-16%), very slight, slight, and slight to strong matrix effervescences, and rare and predominantly few $CaCO_3$ distribution amounts (Table 2; Fig. 4). The uppermost two horizons of the unit were massive while the lower four horizons exhibited weak structural development and many distinct sand primary bedding structures were present in the lowermost two horizons between 9.0 and 9.4 m in depth (Table 2). Sidewall aeolian sand rubification index values (0.51-0.67) and bulk densities (1.59-1.72 g cm^{-3}) showed some variability but were quite similar to values of the overlying GCF (Fig. 4). Dry rupture resistances (0.07-0.27 MPa corresponding to slightly hard, moderately hard, and hard dry resistance classes) and OC (< 0.11%) also exhibited variability throughout the unit but were substantially lower

than values of the GCF (Table 2; Fig. 4). Calcium carbonate equivalent (2.5-6.8%) decreased substantially after the uppermost 3CBkb horizon and exhibited little variability while pH (7.9-8.2) and EC (1.17-3.01 dS m^{-1}) exhibited an inverse relationship and moderate variability throughout the unit (Table 2; Fig. 4). Aeolian sand EC was somewhat similar to that of the overlying GCF and a higher EC value from 8.6 to 9.0 m appeared to indicate increased accumulation of salts as percolation was likely hung up in the 3Bwkb horizon (Table 2; Fig. 4). In addition, HDI (0.21-0.45) of the aeolian sand initially dropped substantially in the uppermost two massive horizons but increased and showed little variability in the four lower horizons of the unit (Fig. 4).

Sangamon Soil

The sidewall section Sangamon Soil unit extended from 9.4 to 10.2 m in depth and exhibited properties consistent with strongly developed horizonation derived from translocation processes modifying Loveland Loess (Table 2). Stronger horizonation was exhibited in two Btkb horizons with a narrow range of moist colors (9.8YR hues; 5.3 values; 3.4-3.7 chromas), clay loam textures (sand range: 36-45%; silt range: 25-35%; clay range: 28-31%), and weak to moderate structural development (Table 2; Fig. 4). The unit also exhibited common distinct clay films (4Btkb1) and few faint clay films (4Btkb2) on ped surfaces, slight to strong matrix effervescences, and few, common, and many $CaCO_3$ distribution amounts (Table 2).

In addition to moist colors, rubification index values (0.42-0.47) of the Sangamon Soil may indicate the presence of reducing conditions in the past as these values were lower than those of the overlying GCF and aeolian sand units (Table 2; Fig. 4). Bulk densities (1.64 g cm^{-3}), OC (< 0.02%), and pH (8.1) showed little variability and were quite similar to values of the overlying aeolian sand unit (Fig. 4). Dry rupture resistances (0.44-2.11 MPa corresponding to

hard dry resistance classes) and CCE (15.8-20.9%) of the sidewall Sangamon Soil exhibited increased variability between the two Btkb horizons with a lower dry rupture resistance but higher CCE for the 4Btkb1 horizon and vice versa for the 4Btkb2 horizon (Table 2; Fig. 4). Sangamon Soil EC (1.08-3.56 dS m^{-1}) also showed increased variability between the two horizons with a higher EC in the 4Btkb1 horizon indicating slowed hydraulic conductivity and increased accumulation of salts in this part of the unit (Table 2; Fig. 4). Horizon development index values (0.55-0.70) of the sidewall Sangamon Soil also showed some variability with a higher value for the 4Btkb1 horizon but, overall, both horizons exhibited stronger soil development when compared to the overlying aeolian sand and underlying Loveland Loess (Table 2; Fig. 4).

Loveland Loess

Loveland Loess of the sidewall section spanned 10.2 to 12.9 m in depth and was composed of a series of Cb and CBwkb horizons (the break between the 4Cb1 and 4Cb2 horizons was arbitrarily broken for descriptions and sampling) exhibiting little to weak soil development with a wider range of moist colors (8.9-9.9YR hues; 4.6-5.2 values; 3.8-4.3 chromas), loam textures (sand range: 39-51%; silt range: 28-39%; clay range: 18-23%) from 10.2 to 12.6 m and sandy clay loam textures (sand range: 49-58%; silt range: 19-26%; clay range: 23-25%) from 12.6 to 12.9 m (Table 2; Fig. 4). All sidewall Loveland Loess horizons were massive with few distinct silt coats on ped surfaces in the 4Cb3 horizon from 11.5 to 11.9 m and many distinct loess primary bedding structures in the 4CBwkb2 and 4CBwkb3 horizons from 12.4 to 12.7 m (Table 2). The massive nature of this unit exhibiting little to weak soil development was also observed and documented in other sites across the Central Great Plains (e.g., Brice, 1966; Feng et al., 1994a; 1994b). The uppermost four horizons of the unit had slight

matrix effervescences and effervescences gradually decreased to very slight to slight, very slight, and noneffervescent for the lower three horizons (Table 2). In addition, rare $CaCO_3$ distribution amounts were present in the 4Cb1, 4Cb2, and 4Cb3 horizons and this increased to few and common $CaCO_3$ distribution amounts in the lower four 4CBwkb horizons (Table 2).

Although sidewall Loveland Loess exhibited little to weak soil development, many of the properties showed a fair amount of variability as rubification index values (0.50-0.88), for the most part, gradually increased with depth and CCE (0.003-9.4%) gradually decreased with depth (Fig. 4). Loveland Loess bulk densities (1.49-1.69 g cm^{-3}) and dry rupture resistances (0.04-0.59 MPa corresponding to soft, slightly hard, moderately hard, and hard dry resistance classes) were quite variable throughout the unit and OC (< 0.36%) increased substantially from surrounding values in the 4Cb2 horizon and especially in the 4Cb3 horizon (Table 2; Fig. 4). The unit also exhibited variability with respect to inversely related pH (7.7-8.7) and EC (0.25-2.81 dS m^{-1}) as higher EC values indicated slowed percolation and increased accumulation of salts throughout parts of the 4Cb2 and 4Cb3 horizons from 11 to almost 12 m and especially throughout the lowermost three horizons (4CBwkb2, 4CBwkb3, and 4CBwkb4) that were overlying pre-Illinoian loess and soils (Table 2; Fig. 4). Horizon development index values (0.13-0.31) of the Loveland Loess were somewhat variable and indicated little to weak soil development in this massive unit (Fig. 4).

Pre-Illinoian Loess and Soils

Sidewall section pre-Illinoian loess and soils spanned approximately 13 to 15 m in depth and were composed of a series of Btkb horizons along with one CBwtkb horizon and this unit showed well-developed horizonation as well as the presence of some massive features (Table 2). The unit exhibited a somewhat narrow range of moist colors (9.3-9.6YR hues; 4.4-5.2 values;

3.7-4.0 chromas) with sandy clay loam textures (sand range: 55%; silt range: 21-24%; clay range: 21-24%) from 12.9 to 13.2 m and clay loam textures (sand range: 37-41%; silt range: 21-31%; clay range: 29-37%) from 13.2 to over 15 m (Table 2; Fig. 4). The unit showed weak, moderate, and strong structural development with massive features present in the 5CBwtkb and 5B'tkb1 horizons (Table 2). The pre-Illinoian unit also exhibited predominantly few and common ped and void surface features, very slight to strong matrix effervescences, and a wide range of $CaCO_3$ distribution (rare, few, common, many, and very many amounts) (Table 2).

Pre-Illinoian unit rubification index values (0.60-0.69), bulk densities (1.66-1.75 g cm^{-3}), and dry rupture resistances (1.46-2.63 MPa corresponding to hard and very hard dry resistance classes) all showed little to moderate variability with rubification index values less than lower parts of the overlying Loveland Loess and bulk densities and dry rupture resistances, for the most part, higher than Loveland Loess values (Table 2; Fig. 4). The unit exhibited slightly more variability with respect to OC (< 0.25%) and CCE (6.0-11.0%) and pH (7.9-8.3), for the most part, gradually increased with depth until slightly decreasing in the lowermost 5B'tkb1 horizon (Fig. 4). Pre-Illinoian unit EC (0.77-3.30 dS m^{-1}) was quite variable with higher values indicating slowed hydraulic conductivity and increased accumulation of salts in the uppermost two horizons and the lowermost horizon overlying the Pierre Shale unit (Fig. 4). As mentioned before, it was unclear why pH and EC exhibited an inverse relationship at this site (Fig. 4). Horizon development index (0.55-0.72) substantially increased from that of the overlying Loveland Loess and continued to gradually increase with depth until slightly decreasing in the lowermost 5B'tkb1 horizon (Table 2; Fig. 4).

Pierre Shale

Pierre Shale of the sidewall section extended from 15 to over 15.5 m and was composed of a Btkb horizon and a Crtk horizon exhibiting properties consistent with residuum soil development (Table 2) similar to that documented in Muhs et al. (1999). These properties included an extremely narrow range of moist colors (9.5-9.7YR hues; 4.3-4.5 values; 3.9-4.0 chromas), a clay loam texture (sand: 35%; silt: 30%; clay: 35%) and weak structural development in the 6Btkb2 horizon, and a clay texture (sand: 31%; silt: 11%; clay: 58%) and massive features in the 6Crtk horizon (Table 2; Fig. 4). The unit also exhibited predominantly few and common ped and void surface features, slight and strong matrix effervescences, and few and many $CaCO_3$ distribution amounts (Table 2). In addition, Ogallala Formation lag gravels were present in the form of few medium pebbles in both horizons and the 6Crtk horizon exhibited saprolitized shale (Table 2).

Pierre Shale unit rubification index values (0.63-0.64), bulk densities (1.69-1.70 g cm^{-3}), dry rupture resistances (2.12-2.54 MPa corresponding to hard and very hard dry resistance classes), and OC (0.02-0.05%) all showed little variability and, for the most part, were quite similar to overlying pre-Illinoian unit horizons (Table 2; Fig. 4). Pierre Shale unit CCE (4.6-14.4%) decreased in the 6Btkb2 horizon from that of the overlying pre-Illinoian unit but subsequently increased in the 6Crtk horizon (Table 2; Fig. 4). Contrasting with this decrease and subsequent increase of the CCE values, pH (8.2-8.4) and EC (4.47-7.23 dS m^{-1}) both increased in the 6Btkb2 horizon from that of the overlying pre-Illinoian unit and then slightly decreased in the 6Crtk horizon (Table 2; Fig. 4). As exhibited in the lowermost 5B'tkb1 horizon of the pre-Illinoian unit, another increase in EC in the 6Btkb2 horizon indicated the continuation of slowed percolation and increased accumulation of salts hung up on and throughout the Pierre Shale unit

(Table 2; Fig. 4). Finally, Pierre Shale unit HDI (0.48-0.65) exhibited a 6Btkb2 horizon value similar to those of the overlying pre-Illinoian unit horizons followed by a substantial decrease in the massive 6Crtk horizon (Table 2; Fig. 4).

Mean Pedostratigraphic Unit Properties and Morphometrics

Rubification Index

Mean rubification index values of the Holocene fill units (headwall: 0.168; sidewall: 0.297) both increased in the Peoria Loess units (headwall: 0.377; sidewall: 0.450) and continued to increase in the GCF (headwall: 0.621; sidewall: 0.631) (Table 3). As expected, rubification index values for the Holocene fill, Peoria Loess, and GCF units not only increased with depth as pedostratigraphy became progressively older and more weathered but values were higher for the sidewall section which had been exposed for a longer time and was more highly weathered. Headwall and sidewall aeolian sand units had mean rubification index values (headwall: 0.613; sidewall: 0.620) that were similar to values of the GCF units but decreased slightly. Sangamon Soil mean rubification index values (headwall: 0.455; sidewall: 0.441) showed substantial decreases from overlying aeolian sand values and appeared to perhaps indicate reducing conditions in the past. Loveland Loess mean rubification index values (headwall: 0.472; sidewall: 0.678) increased from that of the Sangamon Soil units with the headwall value (rubification of one horizon) perhaps continuing to show evidence of reducing conditions and the sidewall value (mean rubification of seven horizons) exhibiting the highest rubification of all of the units indicating substantial exposure and weathering. Sidewall section pre-Illinoian loess mean rubification (0.652) and Pierre Shale mean rubification (0.631) exhibited continued slight decreases from that of the sidewall Loveland Loess but were similar with respect to being more exposed and highly weathered older units.

Table 3. Arithmetic depth weighted mean values of pedostratigraphic properties including dry and moist L*a*b* colors, rubification (Rub), particle-size distribution (PSD), bulk density (BD), organic carbon (OC), calcium carbonate equivalent (CCE), pH, electrical conductivity (EC), and horizon development index (HDI) for the canyon headwall and sidewall. Geometric depth weighted mean values were calculated for dry rupture resistance (RR). Mean values of slope, concavity (Con), and roughness (R) were assessed by pedostratigraphic unit.

Strat†	*N*‡	Dry Color			Moist Color			Rub	PSD			BD	RR	OC	CCE	pH	EC	HDI	Slope	Con	R
		L*	a*	b*	L*	a*	b*		Sand	Silt	Clay										
									———%———			g cm^{-3}	MPa	——%——			dS m^{-1}		%	m^{-1}	m
Headwall																					
HF	4	54.4	5.0	16.9	44.7	5.9	18.2	0.168	39.2	40.6	20.2	1.35	0.10	0.439	3.2	7.6	0.23	0.394	64.0	-0.397	0.197
PL	19	61.5	5.5	19.5	48.8	7.2	21.7	0.377	34.2	47.6	18.2	1.48	0.11	0.185	4.1	8.1	0.22	0.357	52.3	-0.072	0.951
GCF	13	61.5	6.6	19.6	50.2	8.7	23.1	0.621	33.4	35.2	31.4	1.60	2.23	0.137	4.5	7.9	0.75	0.578	63.5	-0.029	0.089
AS	3	60.2	6.8	20.2	52.5	8.5	23.5	0.613	82.9	4.4	12.8	1.71	0.04	0.043	1.8	8.4	0.12	0.230	11.2	0.006	0.163
SSLL	2	68.2	5.3	17.7	56.5	7.7	23.1	0.455	33.1	38.4	28.5	1.72	2.69	0.230	13.1	8.2	0.20	0.670	4.5	0.004	0.065
LL	1	69.4	5.2	18.1	57.6	7.9	23.8	0.472	34.6	45.0	20.4	1.61	0.27	0.092	10.4	8.4	0.21	0.213	NA	NA	NA
Sidewall																					
HF	2	55.0	5.6	18.0	45.4	6.8	20.1	0.297	34.1	44.6	21.4	1.31	0.12	0.641	3.5	7.9	0.20	0.304	29.2	-0.330	0.020
PL	9	62.0	6.0	19.8	52.6	7.5	22.9	0.450	30.8	50.0	19.2	1.47	0.13	0.155	4.8	8.2	0.64	0.194	58.3	-0.091	0.302
GCF	5	60.2	6.5	18.9	50.8	8.6	22.4	0.631	38.6	30.6	30.8	1.65	2.97	0.240	7.1	7.7	2.58	0.612	60.2	-0.076	0.128
AS	6	62.5	6.8	20.1	53.5	8.2	23.0	0.620	76.0	9.9	14.0	1.64	0.13	0.058	3.7	8.1	1.79	0.359	81.2	-0.892	0.291
SSLL	2	68.7	5.2	17.0	53.9	7.4	21.3	0.441	41.1	29.4	29.6	1.64	0.88	0.010	18.6	8.1	2.46	0.634	25.5	-0.044	0.036
LL	7	62.4	7.2	21.2	51.0	9.0	24.2	0.678	46.4	32.2	21.5	1.58	0.27	0.074	4.7	8.3	0.94	0.201	46.2	-0.061	0.146
PI	6	61.1	6.9	20.1	49.5	8.8	23.2	0.652	42.5	27.9	29.6	1.71	1.79	0.051	8.2	8.1	1.29	0.654	32.6	0.068	0.189
PS	2	58.8	7.4	22.0	44.5	9.2	23.9	0.631	33.1	22.3	44.6	1.69	2.35	0.038	8.8	8.3	6.04	0.577	10.1	-0.273	0.065

† Strat, Stratigraphy; HF, Holocene fill; PL, Peoria Loess; GCF, Gilman Canyon Formation; AS, aeolian sand; SSLL, Sangamon Soil formed in Loveland Loess; LL, Loveland Loess; PI, pre-Illinoian loess; PS, Pierre Shale.

‡ *N*, Number of horizons.

Particle-Size Distributions

Mean sand content in the Holocene fill units (headwall: 39.2%; sidewall: 34.1%) decreased in the Peoria Loess units (headwall: 34.2%; sidewall: 30.8%) and these sand contents contributed to loam textures for both Holocene fill units and the headwall Peoria Loess unit and a silt loam texture for the sidewall Peoria Loess (Table 3). Overall, these textures were consistent with weak to moderate soil development as well as massive parts of the Peoria Loess units (Table 2; Table 3). A decrease in mean sand content for the headwall GCF but an increase for the sidewall (headwall: 33.4%; sidewall: 38.6%) contributed to clay loam textures and moderately to strongly developed horizonation for both units with the higher sidewall mean sand content attributed to a lesser amount of sidewall GCF unit horizons due to truncation and removal and a thicker lowermost horizon with a sandy clay loam texture as the unit approached underlying aeolian sand. As expected, mean sand content increased dramatically in the aeolian sand units (headwall: 82.9%; sidewall: 76.0%) and contributed to a loamy sand texture for the massive headwall section unit and a sandy loam texture for the massive to weakly developed horizonation of the sidewall section unit. Mean sand contents of the Sangamon Soil units (headwall: 33.1%; sidewall: 41.1%) contributed to clay loam textures and well-developed horizonation while mean sand contents of the underlying massive Loveland Loess (headwall: 34.6%; sidewall: 46.4%) increased and contributed to loam textures consistent with an overall lack of soil development. The sidewall section pre-Illinoian unit mean sand content (42.5%) and the Pierre Shale unit mean sand content (33.1%) gradually decreased from that of the sidewall Loveland Loess unit and contributed to clay loam and clay textures, respectively, and corresponded with well-developed horizonation and massive parts of these lowermost units.

Mean silt contents of the Holocene fill (headwall: 40.6%; sidewall: 44.6%) contributed to loam textures consistent with weak to moderate soil development (Table 2; Table 3). Increases in mean silt contents occurred in the Peoria Loess units (headwall: 47.6%; sidewall: 50.0%) and contributed to a loam texture for the headwall and a silt loam texture for the sidewall. These mean silt contents contributing to loam and silt loam textures of the Peoria Loess units were consistent with weak to moderate soil development but also corresponded with the massive loess found throughout the units. Substantial decreases in mean silt contents in the GCF units (headwall: 35.2%; sidewall: 30.6%) corresponded to clay loam textures and moderately to strongly developed horizonation. Dramatic decreases in mean silt contents were exhibited in the aeolian sand units (headwall: 4.4%; sidewall: 9.9%) and corresponded with a loamy sand texture and massive features in the headwall and a sandy loam texture and massive to weak soil development in the sidewall. Mean silt contents of the Sangamon Soil units (headwall: 38.4%; sidewall: 29.4%) contributed to clay loam textures and well-developed horizonation and increases in mean silt contents in the Loveland Loess units (headwall: 45.0%; sidewall: 32.2%) contributed to loam textures corresponding with massive features and an overall lack of soil development. Mean silt contents of the sidewall section pre-Illinoian loess (27.9%) and Pierre Shale (22.3%) gradually decreased from that of the sidewall Loveland Loess and corresponded with clay loam and clay textures, respectively, as well as moderately to strongly developed horizonation and massive features in these units.

Holocene fill mean clay contents (headwall: 20.2%; sidewall: 21.4%) contributed to loam textures and weak to moderate soil development while slight decreases in mean clay contents in the Peoria Loess units (headwall: 18.2%; sidewall: 19.2%) corresponded with a loam texture for the headwall and a silt loam texture for the sidewall (Table 2; Table 3). In addition, mean clay

contents of the Peoria Loess units were consistent with weak to moderate soil development and massive loess found throughout the units. Mean clay contents substantially increased in the GCF units (headwall: 31.4%; sidewall: 30.8%) corresponding with clay loam textures and moderately to strongly developed horizonation. A large drop in mean clay contents occurred in the aeolian sand (headwall: 12.8%; sidewall: 14.0%) and was consistent with loamy sand texture and massive features in the headwall section and a sandy loam texture and massive to weak soil development in the sidewall section. Similar to the GCF, substantial increases in mean clay contents also occurred in the Sangamon Soil units (headwall: 28.5%; sidewall: 29.6%) and corresponded with clay loam textures and considerable soil development. Compared to the Sangamon Soil, mean clay contents decreased in the Loveland Loess (headwall: 20.4%; sidewall: 21.5%) and contributed to loam textures consistent with massive features and an overall lack of soil development. Following Loveland Loess of the sidewall section, mean clay content increased in the underlying sidewall pre-Illinoian loess (29.6%) and increased again in the lowermost sidewall Pierre Shale (44.6%) corresponding with clay loam and clay textures, respectively, as well as massive features and considerable soil development.

Bulk Density

Mean bulk densities of the Holocene fill (headwall: 1.35 g cm^{-3}; sidewall: 1.31 g cm^{-3}) were consistent with these units originating as slope wash from upslope Peoria Loess coupled with a relatively short time for soil development (Table 2; Table 3). Increases in mean bulk densities occurred in the Peoria Loess (headwall: 1.48 g cm^{-3}; sidewall: 1.47 g cm^{-3}) corresponding with weak to moderate soil development and massive loess found throughout the units. Additional increases in mean bulk densities occurred in the considerably developed horizonation of the GCF (headwall: 1.60 g cm^{-3}; sidewall: 1.65 g cm^{-3}) and underlying aeolian

sand mean bulk densities (headwall: 1.71 g cm^{-3}; sidewall: 1.64 g cm^{-3}) increased from that of the GCF in the massive headwall section unit but slightly decreased from that of the GCF in the massive to weakly developed sidewall section unit. Compared to the aeolian sand, mean bulk densities of the well-developed Sangamon Soil (headwall: 1.72 g cm^{-3}; sidewall: 1.64 g cm^{-3}) slightly increased in the headwall section and remained the same in the sidewall section. Mean bulk densities decreased in the massive Loveland Loess (headwall: 1.61 g cm^{-3}; sidewall: 1.58 g cm^{-3}) but in the considerably developed horizonation and massive parts of the lowermost two sidewall section units, mean bulk densities increased in the pre-Illinoian unit (1.71 g cm^{-3}) and subsequently slightly decreased in the Pierre Shale unit (1.69 g cm^{-3}). The overall trend of mean bulk densities, for the most part, increasing with depth was in large part likely due to consolidation from the weight of overlying sediments and soils.

Dry Rupture Resistance

Mean dry rupture resistances of the Holocene fill (headwall: 0.10 MPa; sidewall: 0.12 MPa) slightly increased in the Peoria Loess (headwall: 0.11 MPa; sidewall: 0.13 MPa) and these values were consistent with weak to moderate soil development in both units as well as massive features in the Peoria Loess (Table 2; Table 3). Mean dry rupture resistances dramatically increased in the GCF (headwall: 2.23 MPa; sidewall: 2.97 MPa) and corresponded with moderately to strongly developed horizonation. Dramatic decreases in mean dry rupture resistances were exhibited in the aeolian sand (headwall: 0.04 MPa; sidewall: 0.13 MPa) and were consistent with an overall lack of soil development in the massive headwall section unit and massive to weak soil development in the sidewall section unit. Mean dry rupture resistances dramatically increased again in the Sangamon Soil (headwall: 2.69 MPa; sidewall: 0.88 MPa) corresponding with strong soil development with the sidewall section value noticeably lower

most likely due to increased exposure of the upper horizon of the unit to erosion and weathering. Underlying the Sangamon Soil, decreases in mean dry rupture resistances were exhibited in the Loveland Loess (headwall: 0.27 MPa; sidewall: 0.27 MPa) and were consistent with the massive nature of the unit in each section. Lastly, dramatic increases in mean dry rupture resistances were exhibited in the sidewall section pre-Illinoian unit (1.79 MPa) and Pierre Shale unit (2.35 MPa) and were consistent with considerably developed horizonation although some massive features were present.

Organic Carbon

As expected, mean OC contents of the Holocene fill (headwall: 0.44%; sidewall: 0.64%) were higher and decreased in the Peoria Loess (headwall: 0.19%; sidewall: 0.16%) (Table 3). Compared to the Peoria Loess units, mean OC of the headwall section GCF (0.14%) decreased while mean OC of the sidewall section GCF (0.24%) increased. Although OC contents of the GCF noticeably varied due to the cumulic nature of this pedostratigraphic unit, mean OC contents remained low and somewhat similar to the mean OC contents of the less variable Peoria Loess. Predictably, mean OC contents of the aeolian sand (headwall: 0.043%; sidewall: 0.058%) showed considerable decreases to very low values consistent with the loamy sand and sandy loam textures present in the headwall and sidewall sections. Mean OC content of the headwall section Sangamon Soil (0.23%) exhibited an increase but mean OC content of the sidewall section (0.01%) remained very low. Compared to the Sangamon Soil, mean OC contents of the Loveland Loess (headwall: 0.09%; sidewall: 0.07%) were similarly low and consistent with the massive nature of the unit in each section. Lastly, mean OC contents of the sidewall section pre-Illinoian loess (0.05%) and Pierre Shale (0.04%) decreased from that of the sidewall Loveland Loess and remained very low. In summary, with the notable exceptions of the Sangamon Soil in

the headwall section and the GCF in the sidewall section, mean OC contents generally decreased with depth to very low values.

Calcium Carbonate Equivalent

Mean CCE contents of the Holocene fill (headwall: 3.2%; sidewall: 3.5%) were slightly lower but similar to mean CCE contents of the underlying Peoria Loess (headwall: 4.1%; sidewall: 4.8%) and both were consistent with weak to moderate soil development found throughout these units as well as massive features in the Peoria Loess (Table 2; Table 3). Mean CCE contents increased in the moderately to strongly developed horizonation of the cumulic and variable GCF (headwall: 4.5%; sidewall: 7.1%) and were followed by decreases in the aeolian sand (headwall: 1.8%; sidewall: 3.7%) that were consistent with the massive nature of this unit. Mean CCE contents dramatically increased in the strongly developed Sangamon Soil (headwall: 13.1%; sidewall: 18.6%) and subsequently decreased in the underlying massive Loveland Loess (headwall: 10.4%; sidewall: 4.7%). Underlying the sidewall section Loveland Loess unit, mean CCE contents gradually increased in the pre-Illinoian unit (8.2%) and Pierre Shale unit (8.8%) and were consistent with well-developed horizonation and some massive features. Overall, with the exception of the Loveland Loess, mean CCE contents were higher in the sidewall and lower in the headwall most likely corresponding with more weathering and increased pedogenic processes operating over a longer time on the highly exposed sidewall. In addition, mean CCE of the headwall section Loveland Loess unit was determined from only one horizon resting on the canyon floor while mean CCE of the sidewall section Loveland Loess unit was calculated from seven horizons where CCE gradually decreased with depth accounting for the lower mean CCE content in the sidewall.

pH

Holocene fill mean pH values (headwall: 7.6; sidewall: 7.9) were lower than mean pH values of the Peoria Loess (headwall: 8.1; sidewall: 8.2) and the unclear dynamics of the inverse relationship between pH and EC at this site perhaps had a role as higher EC values appeared to indicate some slowed percolation and accumulation of salts hung up in the weak to moderate soil development of the Holocene fill (Table 2; Table 3). The inverse relationship between pH and EC continued into the Peoria Loess as pH fluctuated throughout the weak to moderate horizonation and massive parts of the Peoria Loess, especially in the sidewall section. Once again, these fluctuations were perhaps influenced by higher EC indicating slowed hydraulic conductivity and accumulation of salts although mean pH was typically higher in the Peoria Loess. Decreases in mean pH in the GCF (headwall: 7.9; sidewall: 7.7) were also possibly related to this inverse relationship as higher EC indicative of reduced percolation and increased accumulation of salts occurred throughout the moderately to strongly developed horizonation of the unit. Compared to the GCF, mean pH values of the aeolian sand (headwall: 8.4; sidewall: 8.1) increased and reflected the inverse relationship between pH and EC with respect to most likely readily moving salts through due to increased hydraulic conductivity. This resulted in lower mean EC and higher mean pH although massive to weak soil development in the sidewall section appeared to result in somewhat slowed percolation and increased accumulation of salts.

Compared to the aeolian sand, mean pH values of the Sangamon Soil (headwall: 8.2; sidewall: 8.1) decreased in the headwall section and remained the same in the sidewall section perhaps reflecting reduced hydraulic conductivities and increased accumulation of salts in the well-developed horizonation of the unit in both sections (Table 2; Table 3). Mean pH values of the massive Loveland Loess (headwall: 8.4; sidewall: 8.3) increased from that of the overlying

Sangamon Soil and were consistent with reflecting lower mean EC values corresponding to increased percolation and less accumulation of salts. However, Loveland Loess of the sidewall section exhibited a gradual decrease in pH and increase in EC with depth indicating slowed percolation and increased accumulation of salts as the unit approached underlying pre-Illinoian loess and soils. Compared to the Loveland Loess, mean pH of the pre-Illinoian unit (8.1) in the sidewall section decreased and reflected a higher mean EC corresponding to slowed percolation and increased accumulation of salts throughout considerably developed horizons of the unit. Pierre Shale unit mean pH (8.3) and mean EC (6.04 dS m^{-1}) in the sidewall section both increased from that of the overlying pre-Illinoian unit as the inverse relationship between these properties appeared to not be present despite reduced hydraulic conductivity and increased accumulation of salts in this residuum unit.

Electrical Conductivity

Mean EC values of the Holocene fill (headwall: 0.23 dS m^{-1}; sidewall: 0.20 dS m^{-1}) and Peoria Loess, specifically in the headwall section (0.22 dS m^{-1}), were similar and corresponded with reduced hydraulic conductivity and accumulation of salts throughout the weak to moderately developed soils of these units (Table 2; Table 3). A substantial increase in mean EC in the sidewall section Peoria Loess (0.64 dS m^{-1}) corresponded to reduced hydraulic conductivity and increased accumulation of salts hung up throughout massive parts of this unit. Compared to the Peoria Loess, mean EC of the GCF in the headwall section (0.75 dS m^{-1}) and especially in the sidewall section (2.58 dS m^{-1}) exhibited substantial increases corresponding with moderate to strongly developed horizonation slowing percolation and resulting in increased accumulation of salts. Mean EC of the headwall aeolian sand (0.12 dS m^{-1}) dropped considerably from the overlying GCF as conductivity was likely increased and salts were more easily removed

in this massive unit. Mean EC of the aeolian sand in the sidewall section (1.79 dS m^{-1}) also decreased from that of the GCF but was considerably higher than the mean EC of the aeolian sand in the headwall section due to massive features and weak soil development likely reducing conductivity, slowing the percolation of water, and increasing accumulation of salts.

Mean EC of the headwall section Sangamon Soil (0.20 dS m^{-1}) increased from that of the aeolian sand and corresponded with some slowed percolation of water and a slight increase in accumulation of salts in the well-developed horizonation of this unit (Table 2; Table 3). However, the Sangamon Soil in the headwall section rested on the canyon floor and was clearly highly exposed to erosion and percolation that lowered EC by removing salts. Mean EC of the sidewall section Sangamon Soil (2.46 dS m^{-1}) also increased from that of the aeolian sand and was much higher than mean EC in the headwall section indicating reduced hydraulic conductivity and substantial accumulation of salts in the strongly developed horizonation of this unit. Compared to the overlying Sangamon Soil, mean EC values of the Loveland Loess (headwall: 0.21 dS m^{-1}; sidewall: 0.94 dS m^{-1}) exhibited a slight increase but similar value in the headwall section and a substantial decrease in the sidewall section. The mean EC of the headwall Loveland Loess was similar to the overlying Sangamon Soil due to the previously mentioned increased exposure on the canyon floor as well as the massive nature of the unit. The substantial decrease in mean EC from the Sangamon Soil to the Loveland Loess in the sidewall section was most likely due to increased percolation and removal of salts in this massive unit although EC fluctuated and generally increased with depth as salts accumulated more towards the underlying pre-Illinoian loess and soils. Below the Loveland Loess in the sidewall section, mean EC increased in the pre-Illinoian unit (1.29 dS m^{-1}) and dramatically increased again in the Pierre Shale unit (6.04 dS m^{-1}) as the horizonation of soils in these units reduced hydraulic conductivity

and led to increased accumulation of salts. Lastly, some of the units with higher mean EC values most likely had some horizontal flow of water that resulted in increased accumulation of salts near the faces of the pedostratigraphy exposed in the canyon walls.

Horizon Development Index

Holocene fill mean HDI values (headwall: 0.394; sidewall: 0.304) were consistent with weak to moderate soil development occurring over a relatively short amount of time since deposition of this unit (Table 2; Table 3). Mean HDI values decreased in the Peoria Loess (headwall: 0.357; sidewall: 0.194) as these section units showed weak to moderate soil development but also had large massive parts exhibiting an overall lack of soil development. Compared to the Peoria Loess, mean HDI values of the GCF (headwall: 0.578; sidewall: 0.612) exhibited dramatic increases consistent with moderate to strongly developed horizonation. Following the increases in mean HDI of the GCF, mean HDI values dropped considerably in the aeolian sand (headwall: 0.230; sidewall: 0.359) and were consistent with massive features and an overall lack of soil development in the headwall section and massive to weak soil development in the sidewall section. Mean HDI values dramatically increased again in the Sangamon Soil (headwall: 0.670; sidewall: 0.634) corresponding with strongly developed horizonation. Below the Sangamon Soil, dramatic decreases in mean HDI values in the Loveland Loess (headwall: 0.213; sidewall: 0.201) were consistent with massive features and poor soil development. Lastly, higher mean HDI values in the sidewall pre-Illinoian (0.654) and Pierre Shale (0.577) units corresponded with well-developed horizonation although some massive features were present in both units.

Slope

Mean slopes of the Holocene fill (headwall: 64.0%; sidewall: 29.2%) were considerably different with a higher mean slope for the headwall section corresponding to more active erosion and water shed from all sides of the interfluve nose slope and the lower mean slope of the sidewall section corresponding to more stability as the unit rested upon truncated Peoria Loess (Fig. 2; Table 3). Mean slopes of the Peoria Loess (headwall: 52.3%; sidewall: 58.3%) were representative of the steep interfluve nose slopes common to exposures of massive loess found throughout the Breaks. While the massive and larger exposure of headwall Peoria Loess appeared to shed water quickly on all sides and maintain a steep mean slope, the Peoria Loess in the sidewall section appeared to shed water more slowly with increased percolation yet still maintained a steep mean slope even though hydrological processes were different in these sections. Mean slope of the GCF in the headwall section (63.5%) was similar to the mean slopes of the Holocene fill and Peoria Loess and continued the trend of all three of these units appearing to shed water quickly and maintain steep mean slopes along the headwall interfluve. Mean slope of the GCF in the sidewall section (60.2%) was similar to the headwall section even though hydrological processes were different in these sections as the sidewall was more complex with water shed more slowly and increased percolation. The mean slope of the aeolian sand in the headwall section (11.2%) was gentle as the unit was highly exposed and extended along near the canyon floor as a remnant of ongoing headwall retreat. In contrast to the mean slope of the headwall aeolian sand, mean slope of the aeolian sand in the sidewall section (81.2%) was dramatically higher as the unit was confined between the well-developed and resistant units of the overlying GCF and underlying Sangamon Soil as the sidewall retreated. Although the confined position of the sidewall aeolian sand between the GCF and Sangamon Soil units has

prevented it from being exposed as much, the highly erodible face of the unit has been more exposed and this has resulted in its higher mean slope.

Similar to the headwall aeolian sand, mean slope of the Sangamon Soil in the headwall section (4.5%) was gentle and the unit was highly exposed as it extended along the canyon floor as a remnant of prolonged resistance to ongoing headwall retreat (Fig. 2; Table 3). Mean slope of the Sangamon Soil in the sidewall section (25.5%) was higher than in the headwall section and the sidewall unit was more confined and thicker as it exhibited resistance to erosion and maintained a low slope despite a longer history of exposure to ongoing sidewall retreat. Following the Sangamon Soil in the sidewall section, mean slope increased in the Loveland Loess (46.2%) perhaps corresponding with its properties as massive loess or more likely due to extensive erosion and retreat of the sidewall. Beneath the Loveland Loess in the sidewall section, mean slope decreased in the pre-Illinoian loess (32.6%) and decreased again in the Pierre Shale (10.1%) as these gradually lower mean slopes appeared to correspond with more resistance to erosion and ongoing sidewall retreat.

Concavity

The Holocene fill unit in both sections maintained low mean concavity (headwall: -0.397 m^{-1}; sidewall: -0.330 m^{-1}) due to originating as slope wash that came to rest upon somewhat stable truncated Peoria Loess as water was shed from interfluve nose slopes and into adjacent gullies dissecting the headwall and sidewall (Fig. 2; Table 3). Mean concavity increased in the Peoria Loess (headwall: -0.072 m^{-1}; sidewall: -0.091 m^{-1}) as these massive units shed water into adjacent gullies and maintained steep slopes but were still prone to erosion and removal of parts of interfluve nose slopes resulting in increased concavity. Compared to the Peoria Loess, the GCF exhibited slightly increased mean concavity (headwall: -0.029 m^{-1}; sidewall: -0.076 m^{-1})

consistent with erosion removing parts of the headwall and sidewall sections during retreat. In the headwall section, mean concavity was also influenced by a thicker layer of slope wash and colluvium covering the GCF and resulting in a smoothing effect. Mean concavity of the aeolian sand in the headwall section (0.006 m^{-1}) increased from that of the headwall GCF due to exposure and erosion of the unit as it extended along near the canyon floor. Aeolian sand in the sidewall section exhibited a dramatic decrease in mean concavity (-0.892 m^{-1}) from that of the sidewall GCF because the unit was confined and protected from exposure by the overlying GCF and underlying Sangamon Soil which resulted in a somewhat vertical face susceptible to erosion but maintaining low concavity as well.

Mean concavity of the Sangamon Soil in the headwall section (0.004 m^{-1}) was similar to that of the overlying aeolian sand due to increased exposure and erosion as the unit extended along the canyon floor as a remnant of headwall retreat (Fig. 2; Table 3). Mean concavity of the Sangamon Soil in the sidewall section (-0.044 m^{-1}) increased substantially from that of the sidewall aeolian sand and corresponded with a low mean slope and higher resistance to erosion. Below the Sangamon Soil, mean concavity of the sidewall section Loveland Loess (-0.061 m^{-1}) decreased slightly but was similar to the overlying Peoria Loess, GCF, and Sangamon Soil units; the reason for this similarity may be because all of these units were composed of loess pedostratigraphy subject to a similarly long history of erosion and sidewall retreat. Mean concavity of the pre-Illinoian loess in the sidewall (0.068 m^{-1}) was the highest of all of the sidewall units and corresponded with erosion leveling the unit off and lowering mean slope as it rested near the canyon floor. Lastly, mean concavity decreased in the sidewall section Pierre Shale (-0.273 m^{-1}) as it appeared to be more protected from erosion by the overlying pre-Illinoian loess in addition to being exposed relatively recently at the base of the sidewall.

Roughness

Mean roughness values of the Holocene fill (headwall: 0.197 m; sidewall: 0.020 m) were substantially different with the headwall section exhibiting higher mean roughness due to more active erosion and water shed from all sides of the interfluve nose slope and the lower mean roughness of the sidewall section corresponding with more stability as the unit rested upon truncated Peoria Loess (Fig. 2; Table 3). Mean roughness of the Peoria Loess in the headwall section (0.951 m) increased dramatically from that of the Holocene fill and corresponded with the unit exhibiting massive properties and shedding water quickly but also showing susceptibility to erosion and removal of parts of the headwall interfluve nose slope resulting in increased mean roughness. Likewise, mean roughness of the Peoria Loess in the sidewall section (0.302 m) also increased substantially from that of the Holocene fill and corresponded to the unit exhibiting massive properties and showing susceptibility to erosion and removal of parts of the sidewall interfluve nose slope occurring over a long history of exposure and truncation. Following the increase in mean roughness in the Peoria Loess, mean roughness of the GCF in the headwall section (0.089 m) dropped substantially and corresponded with erosion of a well-developed and resistant unit in addition to increased slope wash and colluvium covering the unit and smoothing the surface. Mean roughness of the GCF in the sidewall section (0.128 m) also decreased from that of the sidewall Peoria Loess and was consistent with erosion of a well-developed and resistant unit subjected to a longer history of exposure and truncation.

Beneath the GCF, mean roughness increased in the aeolian sand (headwall: 0.163 m; sidewall: 0.291 m) and these increases likely corresponded with increased erosion of the unit as it extended near the canyon floor in the headwall section and was confined between the GCF and Sangamon Soil units in the sidewall section (Fig. 2; Table 3). Following the aeolian sand, lower

mean roughness values in the Sangamon Soil (headwall: 0.065 m; sidewall: 0.036 m) corresponded with greater pedogenic development and resistance making the unit less susceptible to erosion. Loveland Loess in the sidewall section showed an increase in mean roughness (0.146 m) consistent with increased susceptibility to erosion occurring over the long history of sidewall retreat. Mean roughness increased in the pre-Illinoian loess of the sidewall section (0.189 m) corresponding to sidewall erosion and retreat leveling off the unit but increasing mean roughness as it extended and rested near the canyon floor. Finally, mean roughness decreased in the sidewall Pierre Shale unit (0.065 m) as it appeared to be more protected from erosion by the overlying pre-Illinoian unit in addition to being exposed relatively recently at the base of the sidewall section.

Pedostratigraphic Unit Property and Landform Relationships

In an effort to analyze pedostratigraphic relationships, depth weighted mean pedostratigraphic property variables (i.e., rubification index, PSD, bulk density, dry rupture resistance, OC, CCE, pH, EC, and HDI) were plotted against mean pedostratigraphic landform variables (i.e., slope, concavity, and roughness) for the headwall and sidewall sections. Based on Pearson product moment correlation coefficients, plots exhibiting the strongest relationships were selected for display if correlation coefficients were significant ($P < 0.1$).

Slope vs. Sand Content

Mean slope for the sidewall section was significantly and positively correlated to mean sand content ($r_S = 0.65$; $P < 0.1$) as this positive correlation appeared to be strongly influenced by the aeolian sand unit (Table 3; Fig. 5). Unlike the aeolian sand in the headwall section, which was highly exposed as it extended along the canyon floor, the aeolian sand in the sidewall section was more confined between the overlying GCF and the underlying Sangamon Soil

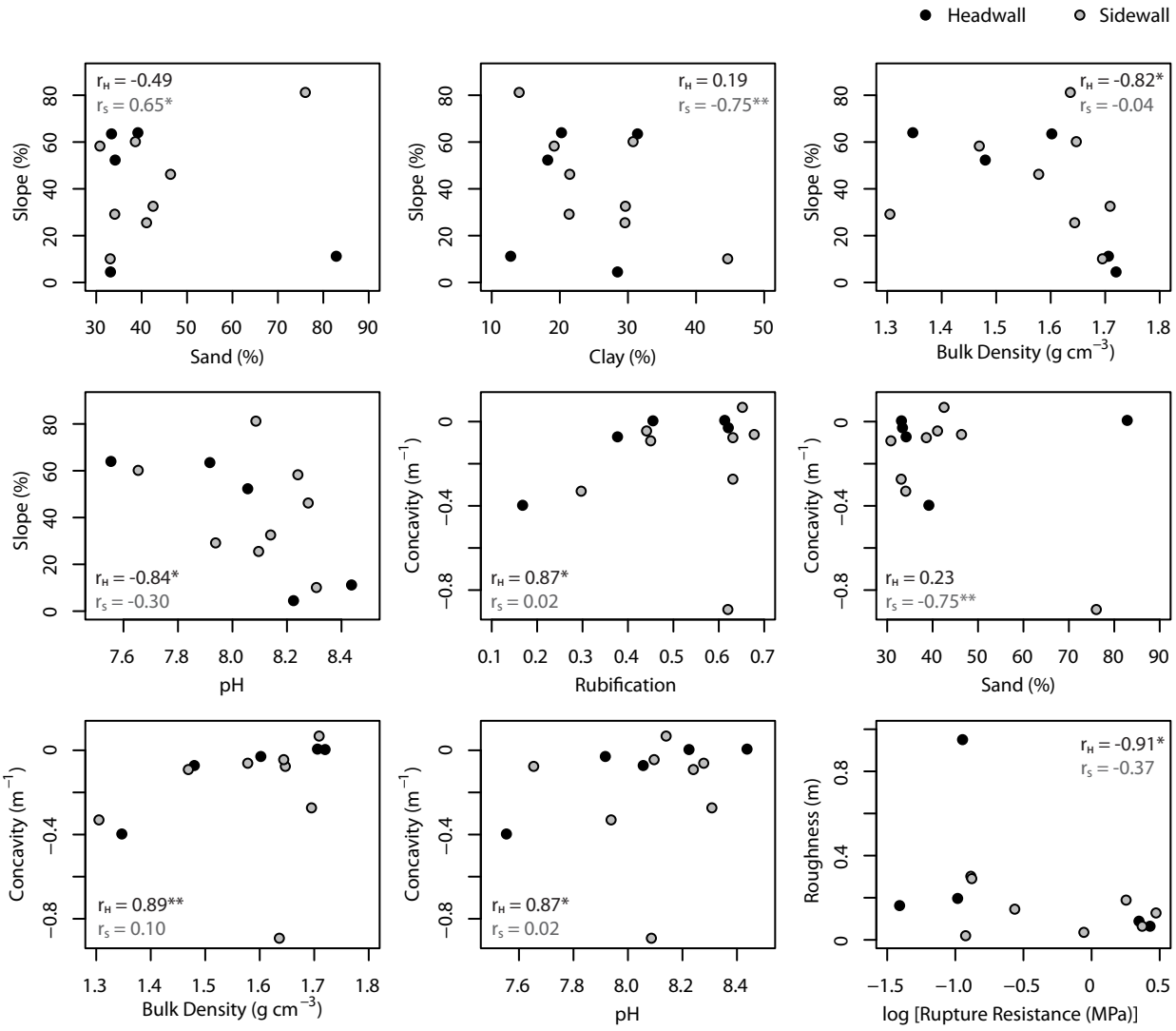

Fig. 5. Pedostratigraphic mean values of slope, concavity, and roughness against depth weighted mean values of pedostratigraphic properties for the headwall (H) and sidewall (S). Pearson product moment correlation coefficients for both headwall and sidewall are displayed on each plot. One or two asterisks represent correlation coefficients that are significant at $P < 0.1$ or < 0.05, respectively. Peoria Loess in the headwall section was excluded as an outlier in the roughness~rupture resistance correlation coefficient calculation.

(Fig. 2). As the sidewall was more exposed to processes of erosion, removal of sediment, truncation, and retreat for a much longer time than the headwall, the more confined position of the aeolian sand unit between resistant pedostratigraphic units (GCF and the Sangamon Soil) resulted in preventing much exposure of the aeolian sand (Fig. 2). However, while the unit was protected from exposure by the overlying GCF and underlying Sangamon Soil units, the exposed and highly erodible face of the aeolian sand unit in the sidewall section has resulted in its higher slope (Fig. 2).

Slope vs. Clay Content

In the sidewall section, mean slope was significantly and negatively correlated to mean clay content (r_S = -0.75; $P < 0.05$) (Table 3; Fig. 5). For the most part, pedostratigraphic units in the sidewall section with higher mean clay contents exhibited more resistance to erosion and had lower mean slopes and vice versa (Fig. 2; Table 3; Fig. 5). With the notable exception of the truncated GCF unit which had a somewhat higher mean slope and higher mean clay content, the Sangamon Soil, pre-Illinoian loess, and Pierre Shale pedostratigraphic units all had higher mean clay contents and lower mean slopes indicative of strong resistance to erosion and sidewall retreat (Fig. 2; Table 3; Fig. 5).

Slope vs. Bulk Density

Headwall section mean slope showed a significantly negative correlation with mean bulk density (r_H = -0.82; $P < 0.1$) (Table 3; Fig. 5). This negative correlation between mean slope and mean bulk density was clearly exhibited in headwall pedostratigraphy as mean slopes, for the most part, decreased with depth and mean bulk densities, for the most part, increased with depth (Fig. 2; Table 3; Fig. 5). A notable exception was the GCF which had a higher mean slope than the overlying Peoria Loess but a mean bulk density that was consistent with other units as far as

increasing with depth (Fig. 2; Table 3; Fig. 5). In addition, the higher mean slope of the GCF was similar to mean slopes of the overlying Holocene fill and Peoria Loess as these units all appeared to shed water quickly while maintaining steep mean slopes along the headwall interfluve (Fig. 2; Table 3). Beneath the GCF, mean slopes decreased dramatically while mean bulk densities increased substantially as these lowermost units (i.e., aeolian sand and Sangamon Soil) extended onto the canyon floor as remnants of headwall retreat (Fig. 2; Table 3; Fig. 5). As mentioned before, the overall trend of mean bulk densities, for the most part, increasing with depth was in large part likely due to consolidation from the weight of overlying sediments and soils.

Slope vs. pH

Pedostratigraphic unit mean slope was significantly and negatively correlated with mean pH in the headwall section (r_H = -0.84; $P < 0.1$) (Table 3; Fig. 5). This negative correlation between mean slope and mean pH was largely related to hydrological processes influencing headwall morphology and an unclear inverse relationship between pH and EC at this site. As previously mentioned, headwall section mean slopes of the Holocene fill, Peoria Loess, and GCF were all somewhat similar and all three of these units appeared to shed water quickly and maintain steep mean slopes along the headwall interfluve (Fig. 2; Table 3). This continuity of steep mean slopes in all three units was in large part due to the massive and vertical nature of the Peoria Loess influencing the overlying Holocene fill and underlying GCF (Fig. 2; Table 3).

However, weak to moderate soil development in the Holocene fill and Peoria Loess units and well-developed horizonation in the GCF unit have had a role in slowing percolation of water and increasing accumulation of salts throughout parts of these units as indicated by higher mean EC values, especially in the GCF (Table 3). Higher mean EC corresponded to lower mean pH in these units as low mean pH appeared to be reflecting accumulation of salts throughout the

headwall pedostratigraphy that perhaps had a role in stabilizing and maintaining steep mean slopes (Fig. 2; Table 3; Fig. 5). Beneath the GCF, mean slope dramatically decreased in the aeolian sand as this highly exposed and eroded unit gently extended onto the canyon floor and was prone to removal of salts and decreased mean EC reflected in increased mean pH (Fig. 2; Table 3; Fig. 5). Similarly, mean slope of the Sangamon Soil remained low as this unit and the underlying Loveland Loess extended as pedostratigraphic remnants onto the canyon floor in positions more exposed to erosion and percolation removing salts and resulting in decreased mean EC reflected in increased mean pH (Fig. 2; Table 3; Fig. 5).

Concavity vs. Rubification

Mean concavity showed a significantly positive correlation to mean rubification in the headwall section ($r_H = 0.87$; $P < 0.1$) (Table 3; Fig. 5). This positive correlation between mean concavity and mean rubification corresponded, for the most part, with both increasing with depth (Fig. 2; Table 3; Fig. 5). Holocene fill in the headwall section originated as reworked Peoria Loess deposited as slope wash and maintained low concavity as the unit rested upon somewhat stable truncated Peoria Loess (Fig. 2; Table 3; Fig. 5). The Holocene fill also exhibited low mean rubification that was consistent with its origin as slope wash but some weak to moderate soil development perhaps slightly increased rubification and likely provided some stability in maintaining low concavity (Fig. 2; Table 3; Fig. 5). Mean concavity increased substantially in the Peoria Loess as this massive unit appeared to shed water quickly into adjacent gullies and maintained a steep mean slope but was still prone to erosion and removal of highly exposed parts of the headwall interfluve nose slope resulting in increased concavity (Fig. 2; Table 3; Fig. 5). Mean rubification of the Peoria Loess also increased from that of the overlying Holocene fill and was consistent with gradual increases in rubification with depth throughout the progressively

older and more weathered massive and weak to moderate horizonation of the unit (Table 3; Fig. 5).

Compared to the Peoria Loess, mean concavity of the GCF unit increased slightly and was consistent with erosion removing parts of the headwall interfluve; mean concavity, however, was also influenced by a thicker layer of slope wash and colluvium covering the unit which smoothed the surface (Fig. 2; Table 3; Fig. 5). Mean rubification continued to increase in the well-developed horizonation of the older and more weathered GCF and this unit marked a transition to more pronounced mean concavity and consistently high mean rubification in the underlying aeolian sand (Fig. 2; Table 3; Fig. 5). Mean concavity of the aeolian sand increased due to increased exposure and erosion of the massive unit as it extended along near the canyon floor (Fig. 2; Table 3; Fig. 5). This increased exposure of the unit also resulted in a high mean rubification value for the aeolian sand as it was exposed for a long time and highly weathered (Fig. 2; Table 3; Fig. 5). Mean concavity of the Sangamon Soil was similar to the overlying aeolian sand as the unit was highly exposed and prone to erosion as it also extended onto the canyon floor as a remnant of headwall retreat (Fig. 2; Table 3; Fig. 5). However, although highly exposed, mean rubification of the Sangamon Soil and the lowermost Loveland Loess decreased from the overlying aeolian sand as mean rubification values for these units appeared to indicate reducing conditions in the past (Table 3; Fig. 5).

Concavity vs. Sand Content

Sidewall section mean concavity was significantly and negatively correlated to mean sand content ($r_S = -0.75$; $P < 0.05$) (Table 3; Fig. 5). Although negative correlations between mean concavity and mean sand content existed for some of the other pedostratigraphic units, this negative correlation was most strongly influenced by the aeolian sand in the sidewall section

(Fig. 2; Table 3; Fig. 5). As previously mentioned, aeolian sand in the sidewall section was confined between the overlying GCF and the underlying Sangamon Soil (Fig. 2). Throughout the long history of sidewall erosion and retreat, the confined position of the aeolian sand between the resistant GCF and Sangamon Soil units resulted in preventing much exposure of the unit except for its highly exposed and erodible face (Fig. 2). This overlying and underlying protection coupled with exposure to the face has resulted in decreased and low mean concavity in the highly erodible aeolian sand unit (Fig. 2; Table 3; Fig. 5).

Concavity vs. Bulk Density

Mean concavity of the headwall section was significantly and positively correlated to mean bulk density ($r_H = 0.89$; $P < 0.05$) and this positive correlation corresponded, for the most part, with both increasing with depth in the pedostratigraphic units (Fig. 2; Table 3; Fig. 5). Holocene fill in the headwall section maintained low mean concavity due to originating as slope wash that rested upon somewhat stable truncated Peoria Loess (Fig. 2; Table 3; Fig. 5). Mean bulk density was also low in this uppermost unit as only weak to moderate soil development was exhibited throughout the fill (Table 3; Fig. 5). Mean concavity increased substantially in the massive Peoria Loess as the unit appeared to shed water quickly and maintained a steep mean slope but was still prone to erosion and removal of highly exposed parts of the headwall interfluve nose slope resulting in increased concavity (Fig. 2; Table 3; Fig. 5). Mean bulk density of the Peoria Loess also increased due to weak to moderate soil development and massive features that were increasingly consolidated from the weight of overlying sediments and soils (Table 3; Fig. 5).

Beneath the Peoria Loess, mean concavity of the GCF increased slightly and was consistent with erosion removing parts of the headwall interfluve but was most likely more

influenced by a thicker layer of slope wash and colluvium covering the unit and smoothing the surface (Fig. 2; Table 3; Fig. 5). As expected, mean bulk density also increased in the GCF due to moderately to strongly developed horizonation and increased consolidation from the weight of overlying sediments and soils (Table 3; Fig. 5). Mean concavity of the aeolian sand increased due to more exposure and erosion of the massive unit as it extended along near the canyon floor (Fig. 2; Table 3; Fig. 5). In addition to erosion and processes of headwall retreat exposing the aeolian sand and increasing mean concavity, mean bulk density of the unit continued to fall in line with increases with depth corresponding to consolidation from the weight of overlying sediments and soils that have now been mostly removed (Fig. 2; Table 3; Fig. 5). Mean concavity of the Sangamon Soil was similar to the aeolian sand as the unit was also highly exposed and extended onto the canyon floor (Fig. 2; Table 3; Fig. 5). Compared to the aeolian sand, mean bulk density of the Sangamon Soil increased slightly corresponding to strong soil development and previous consolidation due to now removed overlying sediments and soils (Table 3; Fig. 5).

Concavity vs. pH

Mean concavity was significantly and positively correlated with mean pH in the headwall section ($r_H = 0.87$; $P < 0.1$) and this positive correlation was related to both variables increasing with depth (Fig. 2; Table 3; Fig. 5). In addition, the positive correlation between mean concavity and mean pH likely reflected the relationship between mean concavity and mean EC as pH and EC were inversely related at this site. As mentioned before, the low mean concavity of the Holocene fill corresponded to its origin as slope wash resting upon truncated Peoria Loess and mean concavity increased in the Peoria Loess due to erosion and removal of highly exposed parts of the headwall interfluve nose slope (Fig. 2; Table 3; Fig. 5). In addition, mean concavity

increased slightly in the GCF and was consistent with erosion removing parts of the headwall interfluve but was also likely influenced by a thicker layer of slope wash and colluvium covering the unit (Fig. 2; Table 3; Fig. 5). Overall, similar to mean slopes, the mean concavity of all three of the uppermost units was in large part due to the massive and vertical nature of the Peoria Loess influencing the overlying Holocene fill and underlying GCF (Fig. 2).

Weak to moderate soil development in the Holocene fill and Peoria Loess and well-developed horizonation in the GCF have had a role in reducing hydraulic conductivity and increasing accumulation of salts resulting in increased mean EC values and decreased mean pH values throughout the units (Table 3; Fig. 5). Although the dynamics of the inverse relationship were unclear, lower mean pH appeared to be reflecting higher mean EC and accumulation of salts throughout headwall pedostratigraphy that may have had a role in stabilizing and maintaining low mean concavities that gradually increased with depth (Fig. 2; Table 3; Fig. 5). Beneath the GCF, mean concavity and mean pH of the aeolian sand both increased as the massive unit was more exposed to erosion and percolation removing salts and lowering mean EC (Fig. 2; Table 3; Fig. 5). Likewise, mean concavity of the Sangamon Soil was similar to the aeolian sand and mean pH of the unit and the underlying Loveland Loess remained higher as these units extended as pedostratigraphic remnants onto the canyon floor in positions more exposed to erosion and percolation that removed accumulation of salts and lowered EC (Fig. 2; Table 3; Fig. 5).

Roughness vs. Dry Rupture Resistance

Pedostratigraphic unit mean roughness was significantly and negatively correlated to mean dry rupture resistance in the headwall section ($r_H = -0.91$; $P < 0.1$) (Table 3; Fig. 5). Mean roughness of the Holocene fill in the headwall section was moderately high due to active erosion

on all sides of the interfluve nose slope (Fig. 2; Table 3; Fig. 5). Although the Holocene fill rested upon and was welded into somewhat stable truncated Peoria Loess, the unit was still prone to erosion and increased roughness as it only exhibited weak to moderate soil development and poor horizonation consistent with low mean dry rupture resistance (Fig. 2; Table 3; Fig. 5). Headwall section Peoria Loess was excluded as an outlier in the mean roughness against mean dry rupture resistance correlation coefficient calculation due to extremely high roughness in an isolated position in the upper part of the unit that was uncharacteristic from the rest of the Peoria Loess roughness along the headwall interfluve (Fig. 2; Table 3; Fig. 5). Although not included as part of the correlation coefficient, the Peoria Loess exhibited high mean roughness and low mean dry rupture resistance as weak to moderate soil development and massive parts of the unit were prone to erosion and removal in highly exposed positions along the headwall interfluve nose slope (Fig. 2; Table 3; Fig. 5).

Beneath the Peoria Loess, mean roughness of the GCF was low and corresponded with high mean dry rupture resistance and reduced susceptibility to erosion in this well-developed, cohesive, and resistant unit (Fig. 2; Table 3; Fig. 5). However, slope wash and colluvium covering the unit have also had a role in lowering mean roughness of the GCF (Fig. 2). Underlying the GCF, mean roughness of the aeolian sand increased and corresponded to low mean dry rupture resistance in this massive unit as well as more exposure to erosion as the unit extended along the canyon floor (Fig. 2; Table 3; Fig. 5). Lastly, mean roughness decreased in the Sangamon Soil and was consistent with mean dry rupture resistance increasing dramatically in this cohesive and strongly developed unit as it extended onto the canyon floor as a remnant of prolonged resistance to headwall retreat (Fig. 2; Table 3; Fig. 5).

Horizon-Scale Property and Landform Relationships

Figures 6, 7, and 8 show cross correlation coefficient values for slope, concavity, and roughness, respectively, versus various soil properties as a function of horizon lag. For reference, negative lags correspond to soil property variables that are associated with landform variables lower in the sections, the distance of which is given by the number of horizons that separate the two variables. Thus, a peak correlation at a horizon lag of -3, for instance, refers to an association between a soil property variable and a landform variable of three horizons below.

Slope vs. Soil Properties

Several of these plots were noteworthy as the headwall section showed positive correlations at negative lag distances for silt (-2), clay (-2), EC (-1), and HDI (-2) suggesting that these properties formed more resistant horizons that acted as caps for underlying nearby layers and allowed the section to steepen downslope (Fig. 6). Increases in silt, clay, and HDI likely resulted in reduced percolation and accumulation of salts increasing EC, thus, furthering resistance to erosion and allowing positions downslope to steepen (Fig. 6). The strong negative correlation at a negative lag distance for sand (-2) supported this interpretation although this negative correlation was likely exaggerated due to increased sand contents in the lowermost two horizons of the GCF and in the highly exposed aeolian sand which extended along near the canyon floor (Fig. 2; Fig. 3; Fig. 6). It was unclear why pH was negatively correlated with slope at a negative lag distance of -1 (Fig. 6). As noted previously, however, pH and EC exhibited an inverse relationship at this site suggesting that the relationship between pH and slope may be more of a reflection of the relationship between EC and slope. Bulk density was negatively correlated with slope at a lag of -1 suggesting that increased bulk density decreases the slope of adjacent horizons downslope although this correlation was likely exaggerated due to units with

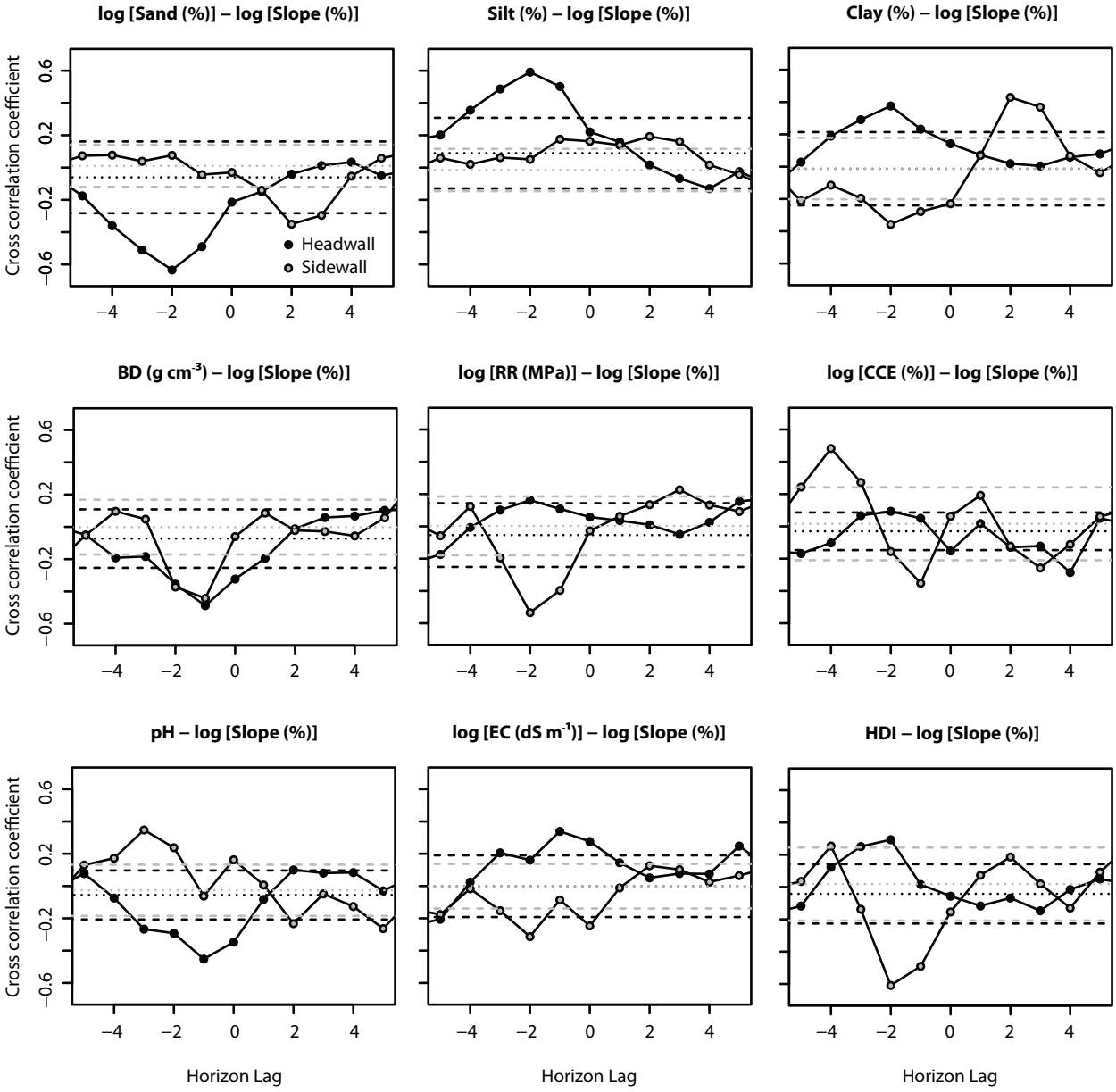

Fig. 6. Cross correlograms for slope versus sand, silt, clay, bulk density (BD), dry rupture resistance (RR), calcium carbonate equivalent (CCE), pH, electrical conductivity (EC), and horizon development index (HDI) for the headwall and sidewall. Black dotted and dashed lines represent the mean and one standard deviation above and below the mean, respectively, for the headwall. Similarly, gray dotted and dashed lines represent the sidewall.

high bulk densities such as the aeolian sand and Sangamon Soil both exhibiting low slopes as they extended onto the canyon floor (Fig. 2; Fig. 6).

Positive correlations were observed in the sidewall section at positive lag distances for silt (2) and more so for clay (2) suggesting that these properties had a role in steepening slopes in upslope positions by forming somewhat stable surfaces on which more highly erodible and, therefore, steep horizons more prone to sidewall retreat rested (Fig. 6). This interpretation was supported by the negative correlation observed at a positive lag distance for sand (2) as decreased sand content increased slope in upslope positions (Fig. 6). In addition to somewhat stable surfaces that more highly erodible and steep horizons rested upon, negative correlations at negative lag distances for clay (-2), bulk density (-1), dry rupture resistance (-2), CCE (-1), EC (-2), and HDI (-2) suggested that these properties combined to form resistant horizons that tended to reduce slope in downslope positions (Fig. 6). As clay, bulk density, dry rupture resistance, CCE, and HDI increased in horizons these properties likely reduced percolation resulting in accumulation of salts increasing EC; as previously mentioned, these properties combined to exert control in reducing slopes in positions downslope (Fig. 6). The positive correlation at a negative lag distance for pH (-3) was consistent with the inverse relationship between pH and EC at this site and likely reflected the relationship between EC and slope (Fig. 6).

Concavity vs. Soil Properties

The headwall section exhibited negative correlations at positive lag distances for silt (2), clay (2), dry rupture resistance (2), and HDI (2) suggesting that these properties formed resistant horizons that had a role in supporting overlying horizons and maintaining lower concavity in upslope positions (Fig. 7). A positive correlation at a positive lag distance for sand (2) further

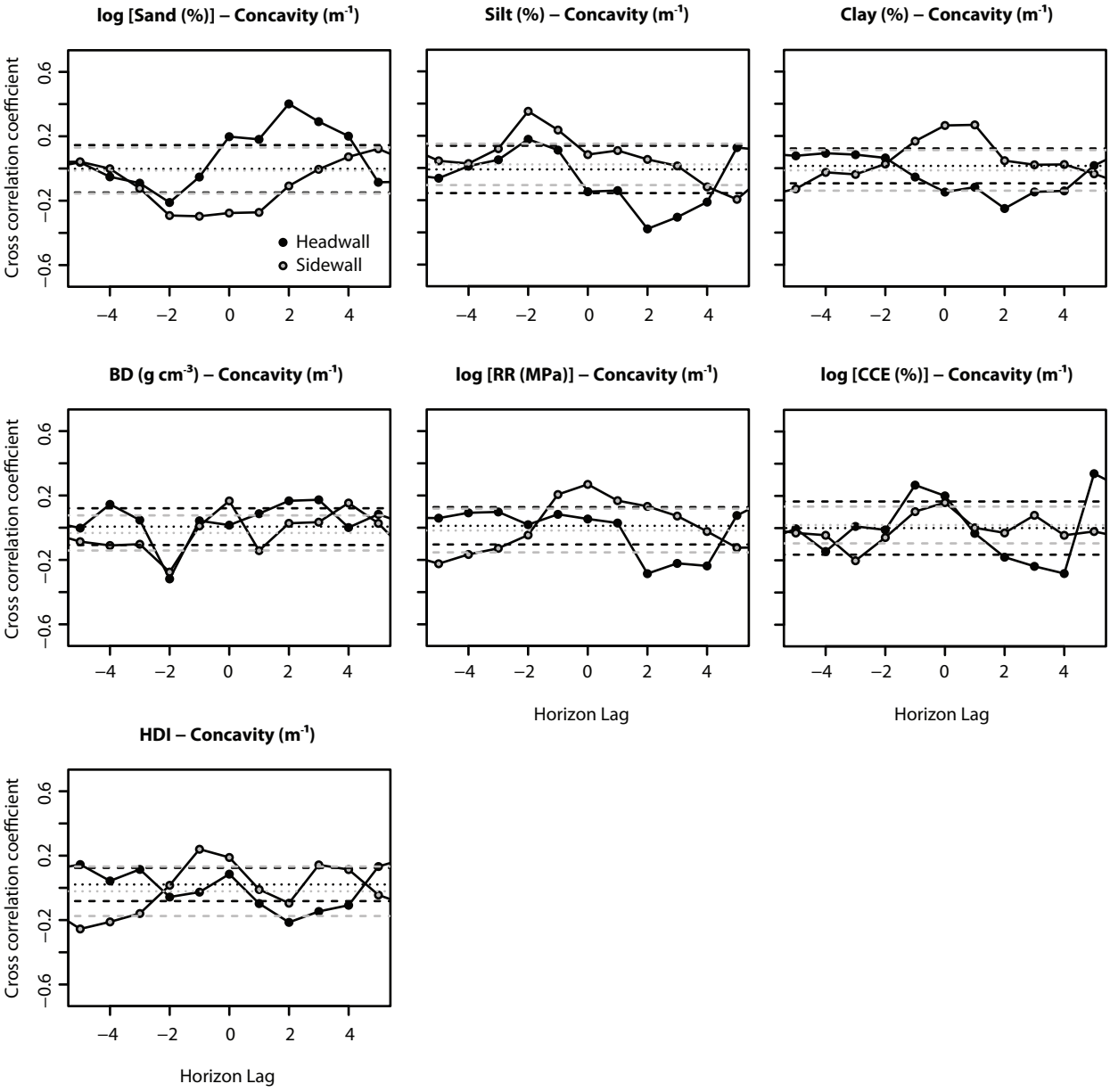

Fig. 7. Cross correlograms for concavity versus sand, silt, clay, bulk density (BD), dry rupture resistance (RR), calcium carbonate equivalent (CCE), and horizon development index (HDI) for the headwall and sidewall. Black dotted and dashed lines represent the mean and one standard deviation above and below the mean, respectively, for the headwall. Similarly, gray dotted and dashed lines represent the sidewall.

supported this interpretation as higher sand content increased concavity in positions upslope due to being more susceptible to erosion although this correlation was likely exaggerated due to the highly exposed aeolian sand unit extending along near the canyon floor (Fig. 2; Fig. 7). The negative correlation at a negative lag distance for bulk density (-2) suggested that higher bulk densities tended to reduce concavity in downslope positions likely by being either more erosive (as with the aeolian sand) or more consolidated (e.g., GCF, Sangamon Soil) which allowed material to be deposited on lower horizons via runoff (Fig. 7). The positive correlation coefficient at a negative lag distance for CCE (-1) suggested that higher CCE increased concavity downslope although this may be overly influenced by gradual increases in concavity with depth and increased CCE in horizons of the GCF and Sangamon Soil units (Fig. 3; Fig. 7).

Positive correlations observed in the sidewall section at lag distances of zero for clay and dry rupture resistance suggested that these properties formed resistant horizons that tended to increase concavity in situ (Fig. 7). Similarly, the positive correlations at negative lag distances for silt (-2) and HDI (-1) suggested that these properties were also components of resistant horizons but rather than exerting as much influence in place, these properties exerted more control in increasing concavity in downslope positions (Fig. 7). The sidewall section exhibited a negative correlation coefficient at a lag of zero for sand suggesting that increased sand content reduced concavity in situ; this negative correlation was likely strongly associated with the resistant GCF capping the aeolian sand and allowing it to maintain low concavity as it was eroded and confined between the GCF and the Sangamon Soil (Fig. 2; Fig. 7). Perhaps related to increased sand content reducing concavity in situ, the negative correlation observed at a negative lag for bulk density (-2) implied that horizons with higher bulk densities tended to reduce concavity in downslope positions likely by being either more erodible (e.g., aeolian sand) or

more consolidated (e.g., GCF, Sangamon Soil) which allowed material to be deposited on lower horizons by runoff (Fig. 7).

Roughness vs. Soil Properties

Negative correlations were observed in the headwall section at lags of zero for clay, dry rupture resistance, EC, and HDI suggesting that these properties formed resistant horizons that tended to reduce roughness in situ (Fig. 8). As previously mentioned, these resistant horizons appeared to reduce percolation that led to accumulation of salts and increased EC and these combined properties formed cohesive horizons that planed smoothly during erosion events therefore reducing roughness in situ (Fig. 8). As noted before, a positive correlation at a lag of zero for pH was consistent with the inverse relationship observed between pH and EC at this site with pH likely reflecting the relationship between EC and roughness (Fig. 8). Similar to clay, dry rupture resistance, EC, and HDI reducing roughness in situ, negative correlations at negative lags for rubification (-2) and silt (-2) implied that these properties were also components of resistant horizons that reduced roughness although this influence was exerted more strongly in downslope positions (Fig. 8). The positive correlation at a negative lag observed for sand (-2) supported this interpretation within the context of higher silt and especially higher clay contents reducing roughness in downslope and in situ positions while higher sand contents tended to increase roughness in downslope positions (Fig. 8). It should be mentioned that the positive correlation between sand and roughness downslope was probably strongly influenced by the increased sand contents in the lowermost two horizons of the GCF and in the highly exposed and erodible aeolian sand unit resting near the canyon floor (Fig. 3; Fig. 8). The positive correlation coefficient at a positive lag distance for silt (3) was likely exaggerated due to uncharacteristically high roughness in isolated and highly exposed upper parts of the Peoria Loess along the headwall

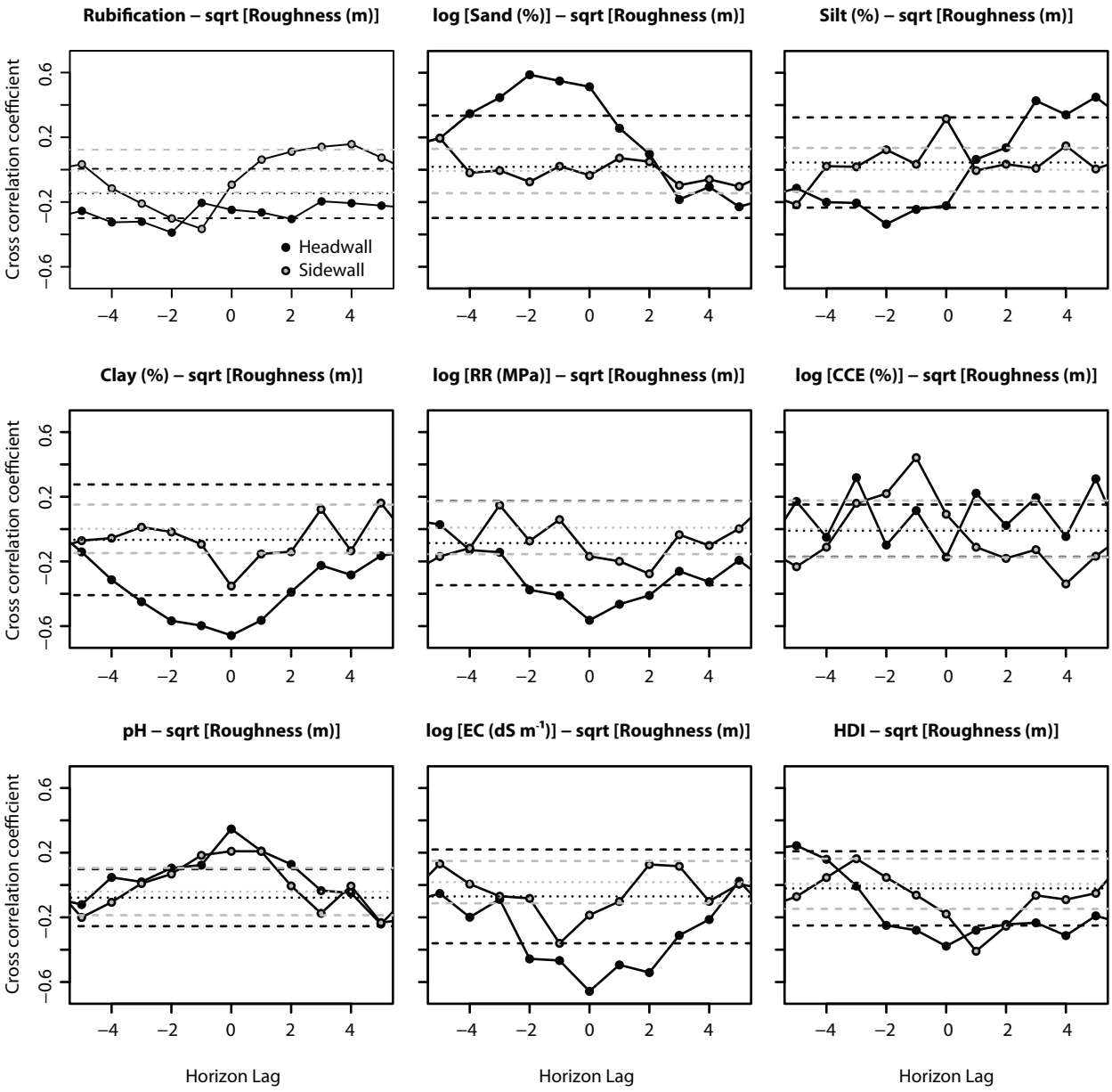

Fig. 8. Cross correlograms for roughness versus rubification, sand, silt, clay, dry rupture resistance (RR), calcium carbonate equivalent (CCE), pH, electrical conductivity (EC), and horizon development index (HDI) for the headwall and sidewall. Black dotted and dashed lines represent the mean and one standard deviation above and below the mean, respectively, for the headwall. Similarly, gray dotted and dashed lines represent the sidewall.

interfluve (Fig. 2; Fig. 8).

The sidewall section exhibited negative correlations at a lag distance of zero for clay and negative lag distances for rubification (-1) and EC (-1) indicating that these properties formed resistant and cohesive horizons that reduced roughness in situ and in downslope positions (Fig. 8). As noted before, these resistant horizons likely reduced hydraulic conductivity resulting in accumulation of salts and increased EC as these properties and processes combined to reduce roughness in situ and in positions downslope (Fig. 8). The positive correlation at a lag distance of zero for pH was consistent with pH being inversely related to EC and likely reflected the relationship between EC and roughness (Fig. 8). Positive correlation coefficients at a lag distance of zero for silt and a negative lag distance for CCE (-1) implied that these properties, in some cases, were components of horizons with lower resistance to erosion and tended to therefore increase roughness in situ and in positions downslope (Fig. 8). Finally, negative correlations observed at positive lag distances for dry rupture resistance (2) and HDI (1) suggested that these properties formed resistant and cohesive horizons that supported overlying horizons and reduced roughness in upslope positions (Fig. 8).

Assessing Relative Importance of Horizon-Scale Properties

For this study, standardized scores of the soil variables were regressed against landform variables to assess the relative importance of the soil variables in influencing the landform variables. Table 4 shows the beta weights and horizon lags of the regressions and Fig. 9 displays plots of measured landform variables against those predicted from the multiple linear regression equations.

Table 4. Beta weights and horizon lags for the multiple linear regression equations used in this study.

y	Statistic	Rub†	Sand	Clay	BD‡	RR§	OC¶	CCE#	pH	EC††	HDI‡‡
					Headwall						
Slope	Estimate		-2.271						-0.521		
	Std. Error		0.570						0.302		
	P		<0.001						0.095		
	Lag		-2						-1		
Concavity	Estimate	5.161	6.983		-8.445						
	Std. Error	1.967	1.805		2.407						
	P	0.014	<0.001		0.002						
	Lag	3	2		-2						
Roughness	Estimate			-0.008			-0.048	-0.107		-0.133	0.151
	Std. Error			0.003			0.027	0.058		0.067	0.112
	P			0.004			0.093	0.077		0.059	0.189
	Lag			0			-1	0		0	0
					Sidewall						
Slope	Estimate	-0.888					-0.263		-0.314		-1.359
	Std. Error	0.423					0.077		0.180		0.316
	P	0.047					0.002		0.094		<0.001
	Lag	-2					-2		-3		-2
Concavity	Estimate			0.171	-6.759	-2.771		0.892	-2.885		7.057
	Std. Error			0.090	3.652	1.354		0.532	1.168		2.350
	P			0.072	0.078	0.053		0.108	0.022		0.007
	Lag			0	-2	0		0	2		-1
Roughness	Estimate					-0.049				-0.080	
	Std. Error					0.022				0.038	
	P					0.037				0.045	
	Lag					2				-1	

† Rub, Rubification.
‡ BD, Bulk Density.
§ RR, Dry Rupture Resistance.
¶ OC, Organic Carbon.
# CCE, Calcium Carbonate Equivalent.
†† EC, Electrical Conductivity.
‡‡ HDI, Horizon Development Index.

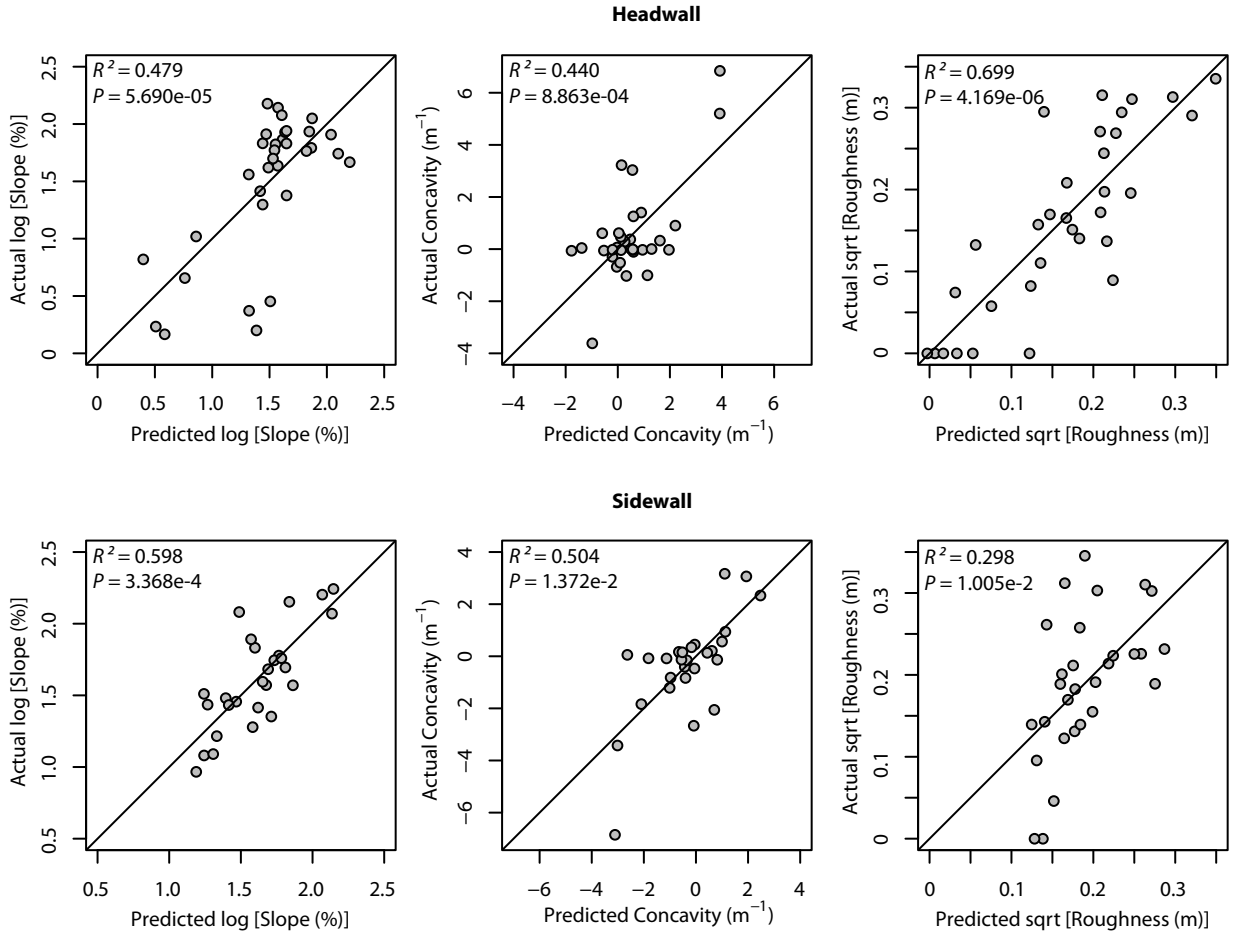

Fig. 9. Actual slope, concavity, and roughness against predicted values from the multiple linear regression equations used in this study.

Headwall Section

Slope of the headwall section was largely explained (R^2 = 0.479) by sand (lag of -2) and pH (lag of -1) (Table 4; Fig. 9). Sand content was the strongest predictor of slope explaining 19.0 times the variation in slope compared to pH, as indicated by the squares of the beta weights (Table 4). As previously mentioned, increased sand content reducing slope in downslope positions was likely exaggerated due to increased sand contents in the lowermost two horizons of the GCF and in the highly exposed and erodible aeolian sand horizons extending with gentle slopes onto the canyon floor (Fig. 2; Fig. 3; Table 4; Fig. 6). As slopes of horizons dramatically decreased in the highly exposed aeolian sand and Sangamon Soil, horizons in these units were prone to erosion and percolation removing salts and decreasing EC and due to the inverse relationship between EC and pH at this site these processes resulted in increased pH of horizons correlating with low slopes in downslope positions (Fig. 2; Table 4; Fig. 6).

Concavity of the headwall section was explained (R^2 = 0.440) by bulk density (lag of -2), sand (lag of 2), and rubification (lag of 3) (Table 4; Fig. 9). Bulk density was the strongest predictor of concavity explaining 1.5 and 2.7 times the variation compared to sand and rubification, respectively, as determined by the squares of the beta weights in Table 4. Sand content explained 1.8 times the variation compared to rubification (Table 4). As mentioned before, horizons with higher bulk densities typically reduced concavity by being either more prone to erosion (e.g., aeolian sand) or more consolidated (e.g., GCF, Sangamon Soil) which allowed material to be deposited in downslope positions via runoff (Table 4; Fig. 7). Increased sand content tended to increase concavity upslope due to being more susceptible to erosion although this positive correlation was likely exaggerated due to the aeolian sand unit horizons extending along near the canyon floor (Fig. 2; Table 4; Fig. 7). Increased rubification also tended

to increase concavity upslope; this positive correlation corresponded to increasing rubification and concavity values with depth as progressively older and more highly weathered horizons gradually transitioned towards increased concavity due to processes of headwall erosion and retreat resulting in remnant horizons extending along the canyon floor (Fig. 2; Table 4).

Horizon development index (lag of zero), EC (lag of zero), CCE (lag of zero), OC (lag of -1), and clay (lag of zero) explained roughness of the headwall section (R^2 = 0.699) (Table 4; Fig. 9). Horizon development index was the strongest predictor of roughness explaining 1.3, 2.0, 9.9, and ~356 times the variation compared to EC, CCE, OC, and clay, respectively, as indicated by squares of the beta weights (Table 4). These results indicated that HDI and EC were primary components of resistant and cohesive horizons that planed smoothly under the influence of erosion and therefore reduced roughness in situ and in positions downslope (Table 4; Fig. 8). As mentioned before, these resistant horizons likely reduced hydraulic conductivity, slowing percolating waters and resulting in the accumulation of salts which increased EC; these properties and processes combined to exert fine-scale control in reducing roughness in situ and in positions downslope (Table 4; Fig. 8).

Sidewall Section

Slope of the sidewall section was explained (R^2 = 0.598) by HDI (lag of -2), rubification (lag of -2), pH (lag of -3), and OC (lag of -2) (Table 4; Fig. 9). Horizon development index was the strongest predictor of slope explaining 2.3, 18.7, and 26.7 times the variation compared to rubification, pH, and OC, respectively, as determined from the squares of the beta weights (Table 4). Rubification explained 8.0 and 11.4 times the variation compared to pH and OC, respectively (Table 4). These results indicated that morphological development (i.e., HDI and rubification index) in the sidewall section largely controlled fine-scale surface slopes in

downslope positions (Table 4; Fig. 6). Horizons with higher HDI and rubification values were more resistant to sidewall erosion and retreat and tended to reduce slopes in positions downslope at this site (Table 4; Fig. 6).

Horizon development index (lag of -1), bulk density (lag of -2), pH (lag of 2), dry rupture resistance (lag of zero), CCE (lag of zero), and clay (lag of zero) explained concavity of the sidewall section (R^2 = 0.504) (Table 4; Fig. 9). Horizon development index was the strongest predictor of concavity explaining 1.1, 6.0, 6.5, 62.6, and ~1703 times the variation compared to bulk density, pH, dry rupture resistance, CCE, and clay, respectively, as indicated by squares of the beta weights (Table 4). Bulk density explained 5.5, 5.9, 57.4, and ~1562 times the variation compared to pH, dry rupture resistance, CCE, and clay, respectively (Table 4). These results showed that HDI was a main component of resistant horizons with higher HDI increasing concavity in downslope positions (Table 4; Fig. 7). Bulk density was also a primary component of horizons influencing concavity as higher bulk densities reduced concavity by being either more erodible (e.g., aeolian sand) or more consolidated (e.g., GCF, Sangamon Soil) which resulted in material being deposited in positions downslope by runoff (Table 4; Fig. 7). Dry rupture resistance was also a key component of resistant horizons exerting influence by increasing concavity in situ (Table 4; Fig. 7).

Roughness of the sidewall section was explained (R^2 = 0.298) by EC (lag of -1) and dry rupture resistance (lag of 2) (Table 4; Fig. 9). Electrical conductivity was the strongest predictor of roughness explaining 2.7 times the variation compared to dry rupture resistance (Table 4). These results suggested that EC and dry rupture resistance were main components of resistant and cohesive horizons that tended to reduce roughness in positions downslope and upslope, respectively (Table 4; Fig. 8). Resistant horizons in the sidewall section likely reduced

percolation resulting in accumulation of salts and increased EC that combined with dry rupture resistance in this case to exert fine-scale control in reducing roughness in downslope and upslope positions (Table 4; Fig. 8).

CHAPTER 4. CONCLUSIONS

This study provides an assessment of the role of both pedostratigraphic unit and horizon-scale variability of soil properties on the development of canyon headwall and sidewall surface slope, concavity, and roughness. It also provides detailed documentation of physical and chemical pedostratigraphic properties as well as pedogenic morphological development of Central Great Plains sediments (loess and sand), soils, and paleosols.

Results indicate that the headwall section of the canyon studied is largely influenced by hydrological processes, which dictate gross-morphology and control slope and concavity much more than pedostratigraphic unit and horizon-scale variability of soil properties. For instance, at the pedostratigraphic unit scale, surface slope and concavity of the headwall section were negatively and positively correlated with bulk density, respectively. Sand content was the strongest predictor of slope at the horizon-scale. These relationships are, however, highly influenced by concentrated hydrological processes that have eroded and exposed lower units (e.g., aeolian sand and Sangamon Soil) causing them to exhibit lower slopes and increased concavity as they extend onto the canyon floor (Fig. 2; Table 5). Bulk density was the strongest predictor of concavity at the horizon-scale as horizons with higher bulk densities tended to reduce concavity likely by being either more erosive (as with the aeolian sand unit) or more consolidated (e.g., GCF, Sangamon Soil) which allowed material to be deposited on lower horizons via runoff (Table 5). However, these processes are likely muted by hydrological processes related to headwall retreat (Table 5). In contrast to slope and concavity, roughness of the headwall section appeared to be more influenced by fine-scale variability of soil properties than by position within the canyon. This was evidenced by HDI being the strongest predictor of roughness at the horizon-scale as higher values indicated cohesion and resistance to erosion and

Table 5. Pedostratigraphic unit (Strat.) and horizon (Hor.) scale correlations (+, positive; −, negative) between soil properties—rubification index (Rub), sand, clay, bulk density (BD), dry rupture resistance (RR), organic carbon (OC), calcium carbonate equivalent (CCE), pH, electrical conductivity (EC), and horizon development index (HDI)—and landform morphometrics—slope, concavity, and roughness for the headwall and sidewall. Pedostratigraphic unit correlations include one or two asterisks indicating significance at $P < 0.1$ or < 0.05, respectively. Based on the multiple linear regression equations and squares of beta weights from this study, horizon-scale correlations with a higher number of + or − indicate stronger predictors of landform morphometrics for either in situ, upslope (🡅), or downslope (🡇) positions.

	Headwall						**Sidewall**					
	Slope		Concavity		Roughness		Slope		Concavity		Roughness	
Property	Strat.	Hor.	Strat.	Hor.	Strat.	Hor.	Strat.	Hor.	Strat.	Hor.	Strat.	Hor.
Rub			+ *	+ + 🡅				− − 🡇				
Sand		− − − 🡇		+ + 🡅			+ *		− **			
Clay						−	− **			+		
BD	− *		+ **	− − − 🡇						− − 🡇		
RR					− *					+ +		− − 🡅
OC						− 🡇		− 🡇				
CCE						− −				+		
pH	− *	− 🡇	+ *					+ 🡇		− − 🡅		
EC						− −						− − − 🡇
HDI						− − −		− − − 🡇		+ + + 🡇		

tended to reduce roughness in situ (Table 5).

In contrast with the headwall, the sidewall section studied has a longer history of exposure and exhibited stronger influence of pedostratigraphic unit and horizon-scale variability of soil properties on surface slope, concavity, and roughness. This influence was observed at the pedostratigraphic unit scale as surface slope was negatively correlated with clay content indicating that units with higher clay contents tended to resist erosion and maintain lower slopes (Table 5). Sand content at this scale was positively correlated with slope and negatively correlated with concavity as these relationships were highly influenced by the aeolian sand unit confined between the more resistant GCF and Sangamon Soil which allowed the unit to maintain a higher slope and lower concavity (Fig. 2; Table 5). At the horizon-scale, pedogenic development (i.e., HDI and rubification index) largely controlled fine-scale surface slopes in downslope positions (Table 5). Horizons with higher HDI and rubification index values exhibited resistance to erosion and retreat and tended to reduce slopes in downslope positions in the sidewall section (Table 5). Horizon development index was also the strongest predictor of concavity at the horizon-scale as higher values indicated resistance to erosion and gradually increased concavity in downslope positions (Table 5). Horizon-scale bulk density was negatively correlated with concavity in downslope positions reflecting similar processes as the headwall where horizons with higher bulk densities tended to deposit material in lower positions through runoff (Table 5). Similar to HDI, horizon-scale dry rupture resistance also had a role in forming resistant horizons with higher values increasing concavity although this influence was predominantly exhibited in situ (Table 5). Finally, results indicated that EC and dry rupture resistance were primary components of resistant and cohesive horizons that tended to reduce roughness in downslope and upslope positions, respectively (Table 5). As mentioned before,

resistant horizons likely had a strong role in reducing hydraulic conductivity which led to accumulation of salts and increased EC that combined with dry rupture resistance to exhibit fine-scale control in reducing roughness in downslope and upslope positions in the sidewall section (Table 5).

The distinctions between primary influences controlling headwall and sidewall morphology and retreat at different scales observed in this study should be taken into account when predicting canyon and gully development (i.e., lengthening and widening) in Central Great Plains sediments, soils, and paleosols. In addition, this research quantified detailed descriptions of soil morphology through the use of development indices such as rubification index and HDI and applied consistence measurements such as rupture resistance to study controls on canyon wall morphology. The measurements and geostatistical approaches (i.e., cross correlograms) adopted in this study should guide future research investigating controls on canyon and gully wall morphology. The relationships studied in this research also provide important information that can be used to inform landscape evolution modeling of canyons and gullies in other areas where thick and highly variable pedostratigraphy is geographically extensive.

REFERENCES

Aleinikoff, J.N., Muhs, D.R., Sauer, R.R., Fanning, C.M., 1999. Late Quaternary loess in northeastern Colorado: Part II—Pb isotopic evidence for the variability of loess sources: Geological Society of America Bulletin 111, 1876-1883.

Aleinikoff, J.N., Muhs, D.R., Bettis, E.A., III, Johnson, W.C., Fanning, C.M., Benton, R., 2008. Isotopic evidence for the diversity of late Quaternary loess in Nebraska: Glacial and non-glacial sources. Geological Society of America Bulletin 120, 1362-1377.

Birkeland, P.W., 1999. Soils and geomorphology. 3rd edition. Oxford University Press, New York.

Blake, G.R., Hartge, K.H., 1986. Bulk density. In: Klute, A. (Ed.), Methods of Soil Analysis, Part 1, Agronomy Monograph 9, 2nd edition Agronomy Society of America, Soil Science Society of America, Madison, WI, pp. 363-374.

Botha, G.A., Wintle, A.G., Vogel, J.C., 1994. Episodic late Quaternary palaeogully erosion in northern KwaZulu-Natal, South Africa. Catena 23, 327-340.

Bouyoucos, G.J., 1962. Hydrometer method improved for making particle size analyses of soils. Agronomy Journal 54, 464-465.

Bradford, J.M., Piest, R.F., Spomer, R.G., 1978. Failure sequence of gully headwalls in western Iowa. Soil Science Society of America Journal 42, 323-328.

Brice, J.C., 1966. Erosion and deposition in the loess-mantled Great Plains Medicine Creek drainage basin, Nebraska. U.S. Geological Survey Professional Paper 352-H, 255-339.

Bryan, R.B., 2000. Soil erodibility and processes of water erosion on hillslope. Geomorphology 32, 385-415.

Bull, L.J., Kirkby, M.J., 1997. Gully processes and modeling. Progress in Physical Geography 21, 354-374.

Chadwick, O.A., Graham, R.C., 2000. Pedogenic processes. In: Sumner, M. (Ed.), CRC handbook of soil science. CRC Press, New York, pp. E41-E73.

Daniels, J.M., Knox, J.C., 2005. Alluvial stratigraphic evidence for channel incision during the Mediaeval Warm Period on the central Great Plains, USA. The Holocene 15, 736-747.

Engleman, E.E., Jackson, L.L., Norton, D.R., 1985. Determination of carbonate carbon in geological materials by coulometric titration. Chemical Geology 53, 125-128.

Eppes, M.C., McFadden, L.D., Matti, J., Powell, R., 2002. Influence of soil development on the geomorphic evolution of landscapes: An example from the Transverse Ranges of California. Geology 30, 195-198.

Feng, Z., Johnson, W.C., Sprowl, D.R., Lu, Y., 1994a. Loess accumulation and soil formation in central Kansas, United States, during the past 400,000 years. Earth Surface Processes and Landforms 19, 55-67.

Feng, Z., Johnson, W.C., Lu, Y., Ward, P.A., III, 1994b. Climatic signals from loess—soil sequences in the central Great Plains, USA. Palaeogeography, Palaeoclimatology, Palaeoecology 110, 345-358.

Frye, J.C., Leonard, A.B., 1951. Stratigraphy of the late Pleistocene loesses of Kansas. Journal of Geology 59, 287-305.

Frye, J.C., Leonard, A.B., 1952. Pleistocene Geology of Kansas. State Geological Survey of Kansas 99.

Harden, J.W., 1982. A quantitative index of soil development from field descriptions. Examples from a chronosequence in central California. Geoderma 28, 1-28.

High Plains Regional Climate Center. 2016. http://www.hprcc.unl.edu (accessed 20 May 2016).

Istanbulluoglu, E., Bras, R.L., Flores-Cervantes, H., Tucker, G.E., 2005. Implications of bank failures and fluvial erosion for gully development: Field observations and modeling. Journal of Geophysical Research 110, F01014.

Jackson, L.L., Roof, S.R., 1992. Determination of the forms of carbon in geologic materials. Geostandards Newsletter 16, 317-323.

Johnson, W. C., Martin, C. W., 1987. Holocene alluvial-stratigraphic studies from Kansas and adjoining states of the east-central Plains. In: Johnson, W. C. (Ed.), Quaternary Environments of Kansas. Kansas Geological Survey Guidebook Series 5, Lawrence, KS, pp. 109-122.

Johnson, W.C., Willey, K.L., 2000. Isotopic and rock magnetic expression of environmental change at the Pleistocene–Holocene transition in the Central Great Plains. Quaternary International 67, 89-106.

Johnson, W.C., Willey, K.L., Mason, J.A., May, D.W., 2007. Stratigraphy and environmental reconstruction at the middle Wisconsinan Gilman Canyon Formation type locality, Buzzard's Roost, southwestern Nebraska, USA. Quaternary Research 67, 474-486.

Kemp, R.A., Zárate, M., Toms, P., King, M., Sanabria, J., Arguello, G., 2006. Late Quaternary paleosols, stratigraphy and landscape evolution in the Northern Pampa, Argentina. Quaternary Research 66, 119-132.

Kirkby, M.J., Bracken, L.J., 2009. Gully processes and gully dynamics. Earth Surface Processes and Landforms 34, 1841-1851.

Knox, J. C., 1983. Responses of river systems to Holocene Climates. In: Wright, H.E., Jr. (Ed.), Late Quaternary environments of the United States 2, The Holocene, University of Minnesota Press, pp. 26-41.

Kukla, G., 1987. Loess stratigraphy in Central China. Quaternary Science Reviews 6, 191-219.

Kukla, G., An, Z., 1989. Loess stratigraphy in Central China. Palaeogeography, Palaeoclimatology, Palaeoecology 72, 203-225.

Logan, M., 2010. Biostatistical design and analysis using R: A practical guide. Wiley-Blackwell, Singapore.

Maat, P.W., Johnson, W.C., 1996. Thermolumescence and new 14C age estimates for late Quaternary loesses in southwestern Nebraska. Geomorphology 17, 115-128.

Mandel, R.D., 1994. Holocene Landscape Evolution in the Pawnee River Valley, Southwestern Kansas. Kansas Geological Survey Bulletin 236, Lawrence, KS.

Mason, J.A., Kuzila, M.S., 2000. Episodic Holocene loess deposition in central Nebraska. Quaternary International 67, 119-131.

Mason, J.A., Jacobs, P.M., Hanson, P.R., Miao, X.D., Goble, R.J., 2003. Sources and paleoclimatic significance of Holocene Bignell Loess, Central Great Plains, USA. Quaternary Research 60, 330-339.

Mason, J.A., Joeckel, R.M., Bettis, E.A., III, 2007. Middle to Late Pleistocene loess record in eastern Nebraska, USA, and implications for the unique nature of Oxygen Isotope Stage 2. Quaternary Science Reviews 26, 773-792.

Mason, J.A., Miao, X., Hanson, P.R., Johnson, W.C., Jacobs, P.M., Goble, R.J., 2008. Loess record of the Pleistocene–Holocene transition on the northern and central Great Plains, USA. Quaternary Science Reviews 27, 1772-1783.

May, D.W., 1992. Late-Holocene valley-bottom aggradation and erosion in the South Loup River Valley, Nebraska. Physical Geography 13, 115-132.

McAuliffe, J.R., 1994. Landscape evolution, soil formation, and ecological patterns and processes in Sonoran Desert bajadas. Ecological Monographs 64, 111-148.

Miao, X., Mason, J.A., Goble, R.J., Hanson, P.R., 2005. Loess record of dry climate and aeolian activity in the early-to mid-Holocene, Central Great Plains, North America. The Holocene 15, 339-346.

Muhs, D.R., Aleinikoff, J.N., Stafford, T.W., Jr., Kihl, R., Been, J., Mahan, S.A., Cowherd, S., 1999. Late Quaternary loess in northeastern Colorado: Part I—Age and paleoclimatic significance. Geological Society of America Bulletin 111, 1861-1875.

Muhs, D.R., Bettis, E.A., III, Aleinikoff, J.N., McGeehin, J.P., Beann, J., Skipp, G., Marshall, B.D., Roberts, H.M., Johnson, W.C., Benton, R., 2008. Origin and paleoclimatic significance of late Quaternary loess in Nebraska: evidence from stratigraphy, chronology, sedimentology, and geochemistry. Geological Society of America Bulletin 120, 1378-1407.

Nettleton, W.D., Olson, C.G., Wysocki, D.A., 2000. Paleosol classification: Problems and solutions. Catena 41, 61-92.

Nielsen, D.R., Wendroth, O., 2003. Spatial and temporal statistics. Sampling field soils and their vegetation. Catena Verlag GMBH, Reiskirchen, Germany.

Olson, C.G., Nettleton, W.D., 1998. Paleosols and the effects of alteration. Quaternary International 51/52, 185-194.

Oostwoud Wijdenes, D.J., Poesen, J., Vandekerckhove, L., Nachtergaele, J., De Baerdemaeker, J., 1999. Gully-head morphology and implications for gully development on abandoned fields in a semi-arid environment, Sierra de Gata, southeast Spain. Earth Surface Processes and Landforms 24, 585-603.

Pelletier, J.D., Quade, J., Goble, R.J., Aldenderfer, M.S., 2011. Widespread hillslope gullying on the southeastern Tibetan Plateau: Human or climate-change induced? Geological Society of America Bulletin 123, 1926-1938.

Pelletier, J., 2012. Fluvial and slope-wash erosion of soil-mantled landscapes: detachment- or transport-limited? Earth Surface Processes and Landforms 37, 37-51.

Poesen, J., Nachtergaele, J., Verstraeten, G., Valentin, C., 2003. Gully erosion and environmental change: importance and research needs. Catena 50, 91-133.

Porter, S.C., An, Z., 2005. Episodic gullying and paleomonsoon cycles on the Chinese Loess Plateau. Quaternary Research 64, 234-241.

Prescott, G.C., Jr., 1953. Geology and ground-water resources of Cheyenne County, Kansas Kansas Geological Survey Bulletin 100, 106 pages.

Pye, K., Winspear, N.R., Zhou, L.P., 1995. Thermoluminescence ages of loess and associated sediments in central Nebraska, USA. Palaeogeography, Palaeoclimatology, Palaeoecology 118, 73-87.

Reed, E.C., Dreeszen, V.H., 1965. Revision of the classification of the Pleistocene deposits of Nebraska. Nebraska Geological Survey Bulletin 23, University of Nebraska Conservation and Survey Division, Lincoln, NE.

Retallack, G.J., 1998. Core concepts of paleopedology. Quaternary International 51/52, 203-212.

Ruhe, R.V., Miller, G.A., Vreeken, W.J., 1971. Paleosols, loess sedimentation and soil stratigraphy. Paleopedology, 41-60.

Schaetzl, R.J., Weisenborn, B.N., 2004. The Grayling Fingers region of Michigan: soils, sedimentology, stratigraphy and geomorphic development. Geomorphology 61, 251-274.

Schoeneberger, P.J., Wysocki, D.A., Benham, E.C., Soil Survey Staff, 2012. Field book for describing and sampling soils, Version 3.0. Natural Resources Conservation Service, National Soil Survey Center, Lincoln, NE.

Schultz, C.B., Stout, T.M., 1945. Pleistocene loess deposits of Nebraska. American Journal of Science 243, 231-244 (671-689).

Simpson, G., Schlunegger, F., 2003. Topographic evolution and morphology of surfaces evolving in response to coupled fluvial and hillslope sediment transport. Journal of Geophysical Research 108 (B6), 2300.

Soil Survey Staff, 2004. Soil survey laboratory methods manual. Soil Survey Investigations Report 42, Version 4.0. Burt, R. (ed.), USDA, Natural Resources Conservation Service.

Soil Survey Staff, 2009. Soil survey field and laboratory methods manual. Soil Survey Investigations Report 51, Version 1.0. Burt, R. (ed.), USDA, Natural Resources Conservation Service.

Tucker, G.E., Arnold, L., Bras, R.L., Flores, H., Istanbulluoglu, E., Sólyom, P., 2006. Headwater channel dynamics in semiarid rangelands, Colorado high plains, USA. Geological Society of America Bulletin 118, 959-974.

USDA, NRCS. 2016. The PLANTS Database (http://plants.usda.gov, 20 May 2016). National Plant Data Team, Greensboro, NC 27401-4901 USA.

Welch, J.E., Hale, J.M., 1987. Pleistocene loess in Kansas—status, present problems, and future considerations. In: Johnson, W.C. (Ed.), Quaternary Environments of Kansas. Kansas Geological Survey, Guidebook Series 5, Lawrence, KS, pp. 67-85.

Willey, K.L., 2009. Environmental and pedogenic change in the Central Great Plains from the Middle Wisconsinan to the present. Ph.D. dissertation, 208 p., University of Kansas, Lawrence.

Wysocki, D.A., Schoeneberger, P.J., LaGarry, H.E., 2000. Geomorphology of soil landscapes. In: Sumner, M. (Ed.), CRC handbook of soil science. CRC Press, New York, pp. E1-E39.

Wysocki, D.A., Schoeneberger, P.J., LaGarry, H.E., 2005. Soil surveys: A window to the subsurface. Geoderma 126, 167-180.